Distribution Category:
Magnetic Fusion Energy
(UC-20)

ANL/FPP/TM-170

ANL/FPP/TM--170

DE83 017538

ARGONNE NATIONAL LABORATORY
9700 South Cass Avenue
Argonne, Illinois 60439

DISCUSSION ON THE CONTROL METHOD OF THE INDUCTOR-CONVERTER BRIDGE BY SIMULATION AND EXPERIMENT

by

Masaru Hirano and Robert L. Kustom

Fusion Power Program

July 1983

Table of Contents

List of Figures

List of Figures (cont.)

List of Figures (cont.)

List of Tables

ABSTRACT

With the development of the superconducting magnet as an energy storage unit, pulsed power loads between superconducting magnets of increasing magnitude up to several hundred megawatts or more appear within the realm of possibility. An energy storage unit that is independent of the power grid can be used in applications where the pulsed power required from the power grid may cause a hazardous effect on the power system. An energy transfer system between the storage and the load units eliminates the disturbance on the power grid. An inductor-converter bridge is proposed for such a purpose.

The inductor-converter bridge (ICB) is a solid state DC-AC-DC converter system for reversible energy transfer between two high-inductance inductors. The converter thyristors are naturally commutated by a set of wye-connected capacitors on the AC lines of the circuit. The circuit is designed so that, in every converter cycle, a very small fraction of the magnet energy is stored in these capacitors. The characteristics of the inductor-converter bridge are briefly summarized as follows: low energy loss, reversibility of the energy transfer direction, controllability of the energy transfer rate, and no conversion to another energy form.

1. Introduction

With the development of the superconducting magnet as an energy storage unit,[1] pulsed power loads between superconducting magnets of increasing magnitude up to several hundred megawatts or more appear within the realm of possibility. An energy storage unit that is independent of the power grid can be used in applications where the pulsed power required from the power grid may cause a hazardous effect on the power system. An energy transfer system between the storage and the load units eliminates the disturbance on the power grid. An inductor-converter bridge is proposed for such a purpose.[2-7]

The inductor-converter bridge (ICB) is a solid state DC-AC-DC converter system for reversible energy transfer between two high-inductance inductors. The converter thyristors[8] are naturally commutated by a set of wye-connected capacitors on the ac lines of the circuit. The circuit is designed so that, in every converter cycle, a very small fraction of the magnet energy is stored in these capacitors. The characteristics of the inductor-converter bridge are briefly summarized as follows: low energy loss, reversibility of the energy transfer direction, controllability of the energy transfer rate, and no conversion to another energy form. The fundamental analysis of the inductor-converter bridge has been contributed by Ehsani.[9]

In Section 3, the dynamic equations are described from the Fourier analysis. Most of the energy is delivered at the fundamental frequency. Using only the fundamental component, we obtain the approximate dynamic equation including the energy loss terms. The dynamic equation describes the system dynamics and provides the methodical background on the modified open-loop control method.

In Section 4, we discuss the performance of the ICB, regulated by the bang-bang control method.[10-13] The bang-bang control method requires a simple control algorithm and keeps a small error signal. We discuss the effect of the voltage swing, relevant to this control method, on the system performance.

In Section 5, a modified open-loop control method is introduced. The equation for this control method is derived from the dynamic equations and contains a complicated function. In order to reduce the execution time for a control computation, we precompute the desired outputs and make a list of the

output values corresponding to each input value and store it in consecutive memory locations. With the aid of the digital microcomputer, the simple control algorithm is obtained.

In Section 6, the frequency modulation method is discussed. Here we explain the performance of the present hardware. Then we describe the technique of implementing the frequency modulation method on the present hardware and discuss its limitation.

In Section 7, we simulate the dynamics of the bang-bang control system and of the feedback control system with frequency modulation. In order to obtain the simulation model, we adjust the error loss terms. In addition to two control methods, a new control method, which combines both methods, is introduced and simulated.

2. System Configuration

Figure 2.1 shows the ICB experimental system. The storage and load units are similarly built with superconducting magnets. In addition, the storage unit contains the current power supply and the thyristor switch that connects the current power supply to the storage unit. The current power supply charges the storage magnet before the energy transfer process starts. Once it starts, the current power supply is disconnected from the energy transfer system due to the back bias on the switch thyristor. Two units are linked by the wye-connected capacitor bank.

Before the energy is delivered from the storage to the load magnets, the storage magnet is charged by the current power supply through the switched-on thyristor, SS7. In the meantime, the two capacitors, C_1 and C_3, are also charged by their parallel-connected voltage power supplies, PS2 and PS3, respectively. The magnitude, $|V_o|$, of the initial capacitor voltage is

$$|V_o| = \frac{I_o T}{6C}$$

where I_o is the initial value of the storage current and T is the converter period. The polarities of the two capacitors are opposite, shown as the sign on each capacitor in Fig. 2.1. The resistors, R_2 and R_3, reduce the current flow through the power supplies, PS2 and PS3, during the energy transfer period. At the beginning of the energy transfer period, the thyristor does

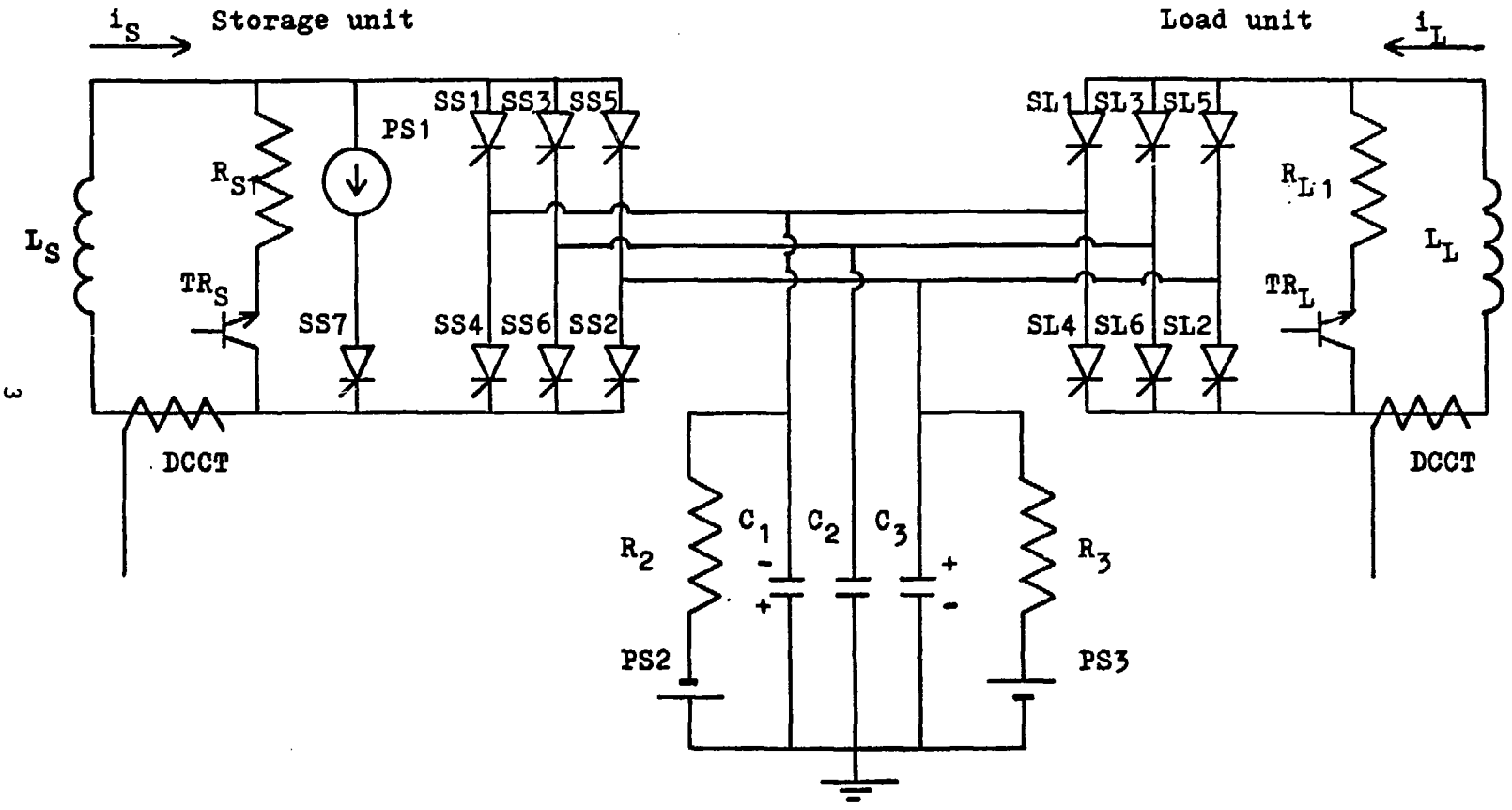

Fig. 2.1. ICB experimental system.

not obtain enough hold current in the uncharged, high inductance magnet because of the slow current rise. When either unit carries a low current, the power transistor on its side is switched on and the resistor, R_{S1} or R_{L1}, conducts enough current to hold the thyristor on. The firing of the power transistor is executed by the computer control sequence.

The energy transfer rate is controlled by the phase between two switching sequences. The phase difference is defined as the phase by which the load side switching sequence leads the storage side. The thyristor gates are fired in the order shown by its thyristor number. At first, the thyristors with numbers 1 and 2 in each bridge are switched on at the same time. Then the phase difference is moved from zero degree to the desired value. In order to keep the capacitor voltages in balance after phase difference or converter frequency shift, the trigger pulse sequence complies with the three-step or four-step transient shifting technique explained in Section 6.

Tables 2.1 and 2.2 show the characteristics of the superconducting magnet and the thyristor, respectively. Table 2.3 shows the other parameters in the experimental system.

Table 2.1 Characteristics of the Superconducting Magnet

Dimensions:	
Outer Diameter	11 in.
Inner Diameter	8 in.
Length	18 in.
Conductor:	
Inductance	4 H
Critical Current	265 A
Composition	NbTi
Stabilizer	Copper
Cooling Type	Pool Cooling

Table 2.2 Characteristics of the Thyristor

Type	IT - 151RF30
Maximum Repetitive Off-State Voltage (VDRM)	300 V
Maximum Static On-State Current (IT)	235 A
Maximum Hold Current	200 mA
Maximum On-State Voltage	1.9 V
Typical On-Switching Time	300 μsec
Typical Off-Switching Time	20 μsec
Rise Rate of Recovery Voltage	200 V/μsec

Table 2.3 System Parameters

Power Supplies	
PS1:	
Maximum Voltage	100 V
Maximum Current	100 A
PS2 and PS3:	
Maximum Voltage	150 V
Resistors	
R_S and R_L	250 Ω
R_3	10 kΩ
Capacitors	
C1, C2, and C3	200 μF
DC Current Transformer	
Rated Current	± 250 A dc
Rated Output (RO)	± 10 V dc
Response Time to 99%	< 150 μsec
Linearity	< ± 0.5% RO

Table 2.4 Features of the Microcomputer and the A/D Converter

Microcomputer	
CPU	8080 A
Resolution	8 bit
Clock Rate	1M Hz
Memory Size:	
PROM	2K byte
RAM	34K byte
Additional:	
- Eight-level interrupt	
- 48 lines of parallel I/O programmable for unidirectional input/output or bidirectional ports	
A/D Converter	
Resolution	12 bits
Number of Channels	16 ports
Rated Input	± 10 V Bipolar
Type of Output	Two's complement
Total Conversion Time	33 μsec
System Accuracy	± 0.025 % FSR

Figure 2.2 shows the microcomputer and its interfaces. Table 2.4 shows the features of the microcomputer and the A/D converter. The storage and load currents, i_S and i_L, are detected by the dc current transformers (DCCT). The reference signal, i_R, is supplied from the function generator. The converter frequency, f, and the phase difference, ϕ, can be manually adjusted by the rotary switches on the external control board. Each analog signal is connected to its assigned input port of the multiplexer and converted into a digital value by the A/D converter. The digital values of the converter frequency and the phase difference are shown on the external LED display. The interrupt signal from the pulse sequencer is only accepted during the transient period of the phase or the frequency shift. In other cases, the interrupt mask prevents the interrupt signal from interfering the control command sequence.

At the Argonne National Laboratory, the source program is compiled by the 8080A cross assembler on the IBM interactive system, CMS. The object program is punched out on the paper tape and loaded from the tape reader of the teletypewriter (TTY) to the microcomputer memory. The program, MONITOR, in the PROM controls the tape loading process and provides the access to the editing of the computer memory contents.

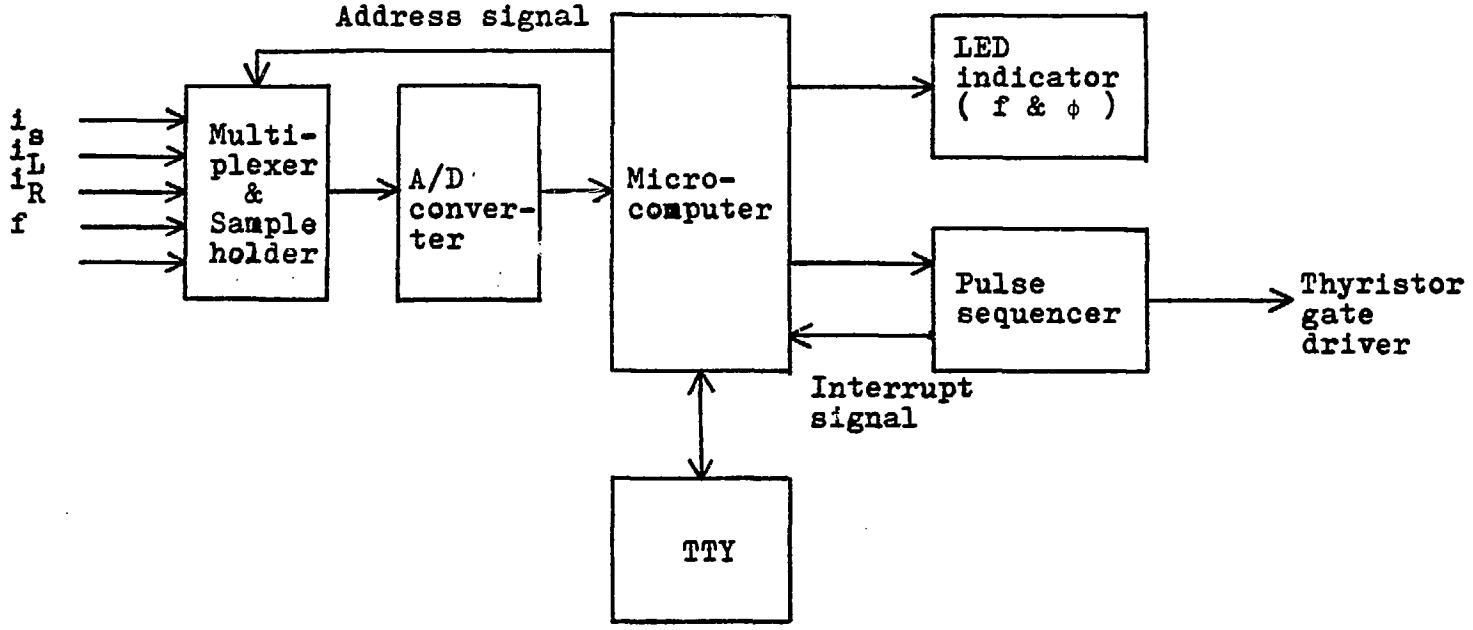

Fig. 2.2. Block diagram of the microcomputer and its interface.

3. Mathematical Description of the Inductor-Converter Bridge

Figure 3.1 shows the block diagram of the energy transfer process. The energy is drained from the storage unit and accumulated in the load unit. Two six-pulse thyristor converters separate the storage and the load units from the capacitor bank. The storage side thyristors act as an inverter to transform dc power in the storage unit to ac power in the capacitor bank, while the load side thyristors rectify the ac power in the capacitor bank to produce dc power in the load unit. The power of the capacitor bank is equal to the power flow from the storage unit and to the power flow to the load unit as far as loss is negligible.

The capacitor voltage waveform is formed by the current flow from the two units to the capacitors and can be varied during the energy transfer period. The capacitors in the bank are initially charged in order to maintain the balance of the capacitor voltage waveform after the energy transfer starts. During the shifting of phase difference, frequency, or both, the capacitor voltages cannot keep the balance of their waveform because of the different switching interval in each phase. The shifting technique, described in Section 6, restores the balance of the capacitor voltage waveform after the shifting period.

The converter frequency can be regulated and its range can be widely varied because the ICB is independent of the power grid. At a low frequency, energy in the capacitor bank in a converter cycle is increased and a large capacitor size is required. In addition, the low frequency provides the high magnitude of the capacitor voltage, so that the switching voltage is increased. The ultimate voltage is restricted by the thyristor or capacitor breakdown voltage. Therefore, the lower limit of the converter frequency is determined by the capacitor size and the thyristor characteristics. High frequency is limited by the turn-on and -off speeds of the thyristor, so that a relatively high frequency can be available for the ICB. The frequency range in our system can be varied from 430 to 7K Hz.

The phase difference determines the energy transfer rate and its direction. Energy is delivered from the storage to the load magnets for the positive phase difference and conversely for the negative one. The operation range of the phase difference is varied with the current ratio, but average power maintains maximum for each current ratio when the phase difference is

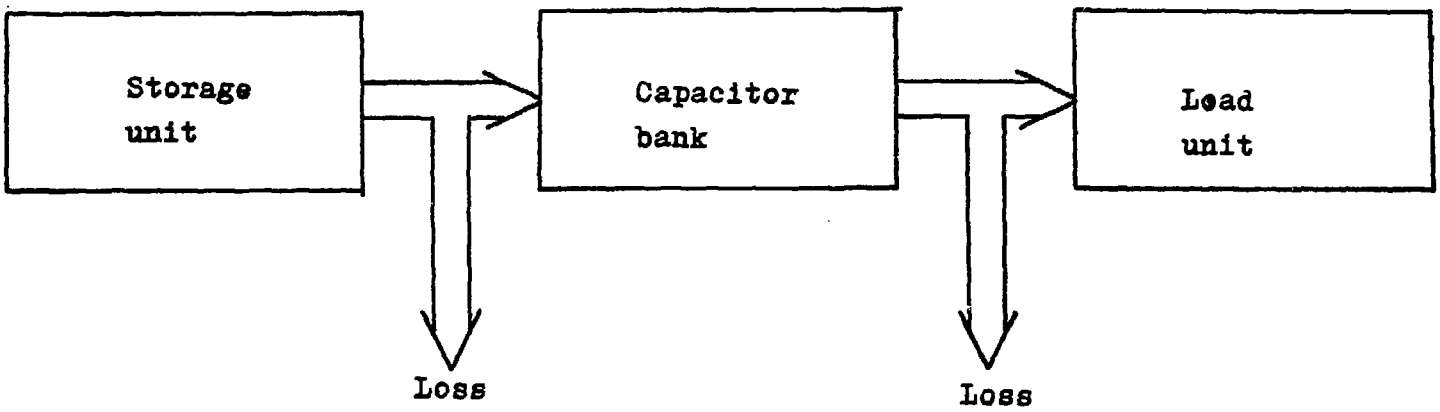

Fig. 3.1. Block diagram of the energy transfer process.

equal to + 90°. The reversed direction of power flow is also maximized for each current ratio when the phase difference is equal to - 90°.

Power in the capacitors can be calculated as follows: The mathematical expression of the capacitor current waveform, that is, a square waveform, is expressed as a Fourier series. The capacitor voltage is the integral of the sum of the two component currents, divided by the capacitance. Then the power of one capacitor is the product of the capacitor current and voltage. Power, P(t), is approximately given by neglecting higher harmonics:[2]

$$P(t) = \frac{54\, i_S(t)\, i_L(t)\, t_{sw}}{\pi^3 C} \sin \phi \,, \tag{3.1}$$

where $i_S(t)$ and $i_L(t)$ are the storage and the load currents, respectively, and ϕ is the phase difference.

The power from the storage magnet supplies the power of the capacitor bank and the loss. On the other hand, power from the capacitor bank provides power to the load magnet and the loss. The loss takes place due to the wiring resistance, the thyristor forward voltage, and the thyristor switching circuit losses. The resistive loss and the thyristor forward voltage drop can be easily expressed in terms of the storage and the load currents. But the thyristor switching loss is difficult to express because of its dependence on many factors such as the switching voltage and current, the converter frequency, the impedance in the commutation circuit, the turn-off time of the thyristor, and the snubber circuit parameters. Then the power flow can be described as follows:

$$-\frac{d}{dt}\left(\frac{L_S i_S^2(t)}{2}\right) = P(t) + 2V_f i_S(t) + R_S i_S^2(t) \,, \tag{3.2}$$

$$\frac{d}{dt}\left(\frac{L_L i_L^2(t)}{2}\right) = P(t) - 2V_f i_L(t) - R_L i_L^2(t) \,, \tag{3.3}$$

where V_f is the thyristor forward voltage, and R_S and R_L are the wiring resistances in the storage and the load sides, respectively.

After some manipulation, the dynamic equations are obtained as follows:

$$\frac{di_S(t)}{dt} = -\frac{54\ t_{sw}\ \sin\phi}{\pi^3 L_S C}\, i_L(t) - \frac{R_S}{L_S}\, i_S(t) - \frac{2V_f}{L_S}\ , \tag{3.4}$$

$$\frac{di_L(t)}{dt} = \frac{54\ t_{sw}\ \sin\phi}{\pi^3 L_L C}\, i_s(t) - \frac{R_L}{L_L}\, i_L(t) - \frac{2V_f}{L_L}\ . \tag{3.5}$$

The phase difference, ϕ, and the switching interval, t_{sw}, can be varied as the control parameters. The two state variables, $i_S(t)$ and $i_L(t)$, are solved by the two dynamic equations with the time-variable coefficients. In a simulation, we can obtain the system dynamics by changing the coefficients at each iteration. Therefore a small time step is required for an accurate result.

4. Bang-Bang Control Method

The bang-bang control method, one of the nonlinear control methods, has been chosen as the first controller of the feedback control system for the ICB. This method may be very effective for a system where there exists a pole near the origin on the s-plane. The ICB fits this case because of its superconducting magnet with a large inductance and its small wiring resistance. When a feedback control method with a linear controller is applied to this kind of system, the control system may hardly keep a small value of an error signal. The bang-bang control method provides the two extremes of control action according to the sign of the error signal. Then the bang-bang controller responds to the change of polarity of the error signal so sensitively that it keeps a small value of the error signal.

Figure 4.1 shows the block diagram of the control system for the ICB. Here, $i_R(t)$ is the instantaneous reference signal and $i_L(t)$ is the instantaneous load current. In this strategy, the operating phase difference is switched from one extreme, $-90°$, to the other, $+90°$, according to the sign of the error quality, $i_R(t) - i_L(t)$, at any given time. The bang-bang control strategy renders no decision for the singularity case of $i_R(t) - i_L(t) = 0$. The swing of the phase difference changes the polarity of the magnet voltage; in other words, the energy transfer direction is reversed. However, the total power flow follows the direction given by the reference signal.

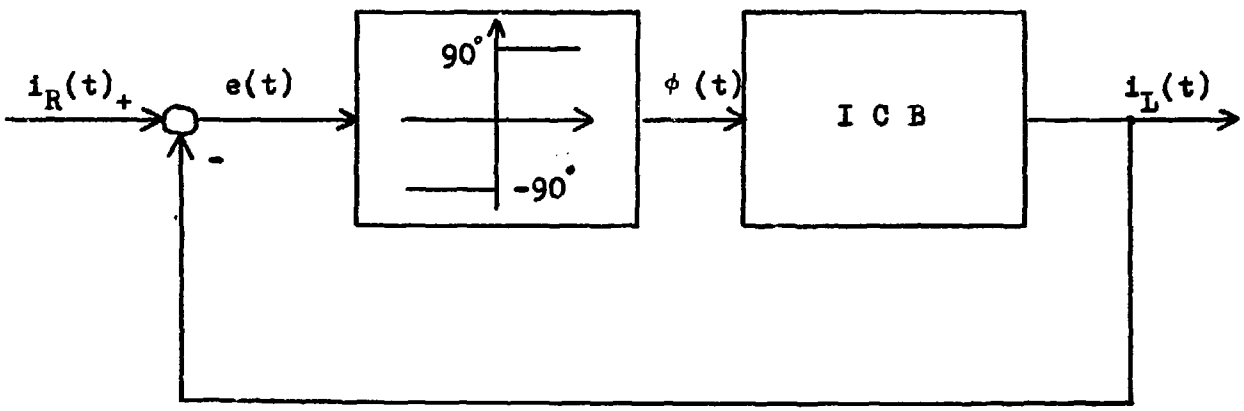

Fig. 4.1. Control system with the bang-bang control method.

Figures 4.2 and 4.3 show the experimental results of the bang-bang control method with and without a 1kHz low pass filter located between the dc current transformer (DCCT) and the A/D converter. The filter eliminates the noise on the feedback signal. The data curves shown from top to bottom of the chart are the reference signal, storage current, load current, storage voltage, and load voltage.

When the reference signal crosses the zero axis, the energy is delivered from the storage to the load magnets. The storage magnet is initially charged with a current of 100 A wye-connected capacitor bank in the ac lines of the circuit stores a small fraction of the magnet energy at the frequency of 1157 Hz. The reference signal is generated in such a way that the load current waveform is characterized by two intervals: a charging and a discharging period with constant rate of the current rise of 15 and - 15 A/sec, respectively. The load current moves in each quantization band, determined by the resolution of the A/D converter and the microcomputer. The quantization band is characterized as a region where a digital signal does not respond to the change of the real signal. The dc voltages in the storage and the load sides swing over the positive and negative maximum values. Some of the high frequency components of the voltage oscillation may be lost because its frequency exceeds the bandwidth of the pen recorder. As compared with the dc voltage waveforms in Figs. 4.2 and 4.3, the existence of noise can be recognized. Figure 4.4 shows the waveform of the signals, which corresponds to the storage and load currents and which is detected by the DCCT. The upper and the lower signals correspond to the storage and the load currents. The abscissa is drawn on the waveform of the load current so that this signal waveform may not be clearly distinguished from the abscissa. Two waveforms of Fig. 4.4 have the following characteristics: they consist of an oscillation synchronized with the converter frequency and a pulse-type ripple with high magnitude. The former oscillation is due to the imbalance of the capacitance in the three-phase capacitor bank and of the initial capacitor voltage. The latter pulse-type ripple is due to the thyristor switching. We have to remove the pulse-type ripple which appears as noise. This pulse has a higher frequency than the converter frequency so that the low pass filter can eliminate it without changing the waveform of the fundamental signal. The constant inverval of the voltage oscillation can be shown in the experiment where the filter is installed. The number of the voltage oscillation depends on the

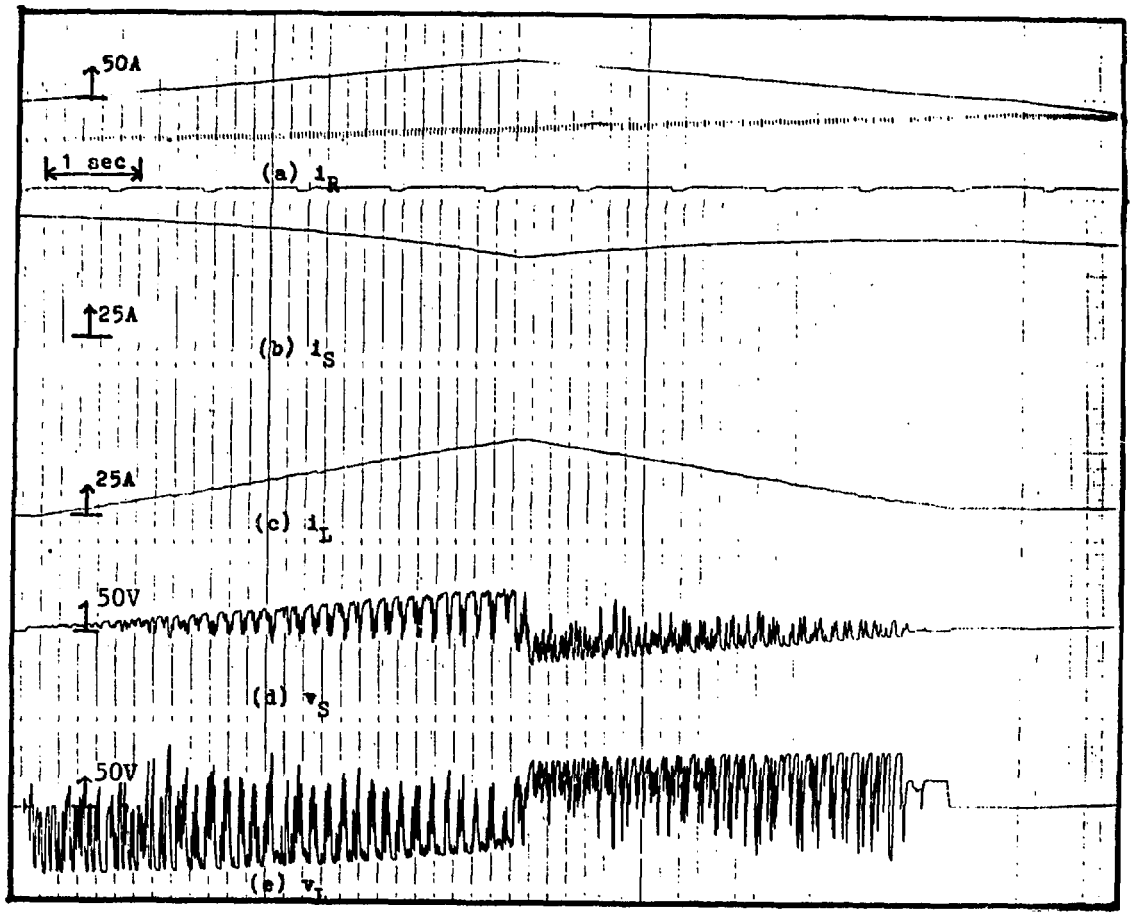

Fig. 4.2. Experimental result by the bang-bang control method without the filter, where i_R is the reference signal, i_S is the storage current, i_L is the load current, v_S is the storage voltage, and v_L is the load voltage.

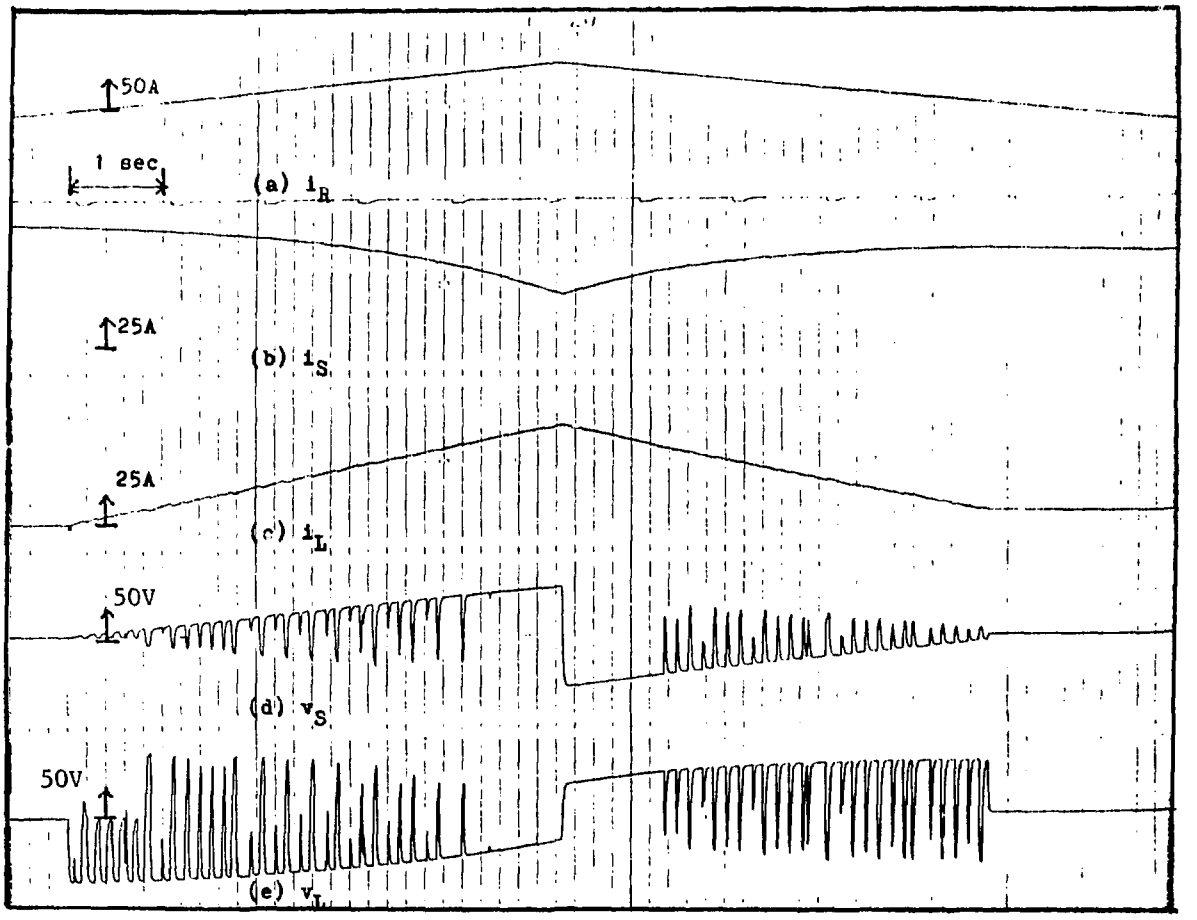

Fig. 4.3. Experimental result by the bang-bang control method with the filter, where i_R is the reference signal, i_S is the storage current, i_L is the load current, v_S is the storage voltage, and v_L is the load voltage.

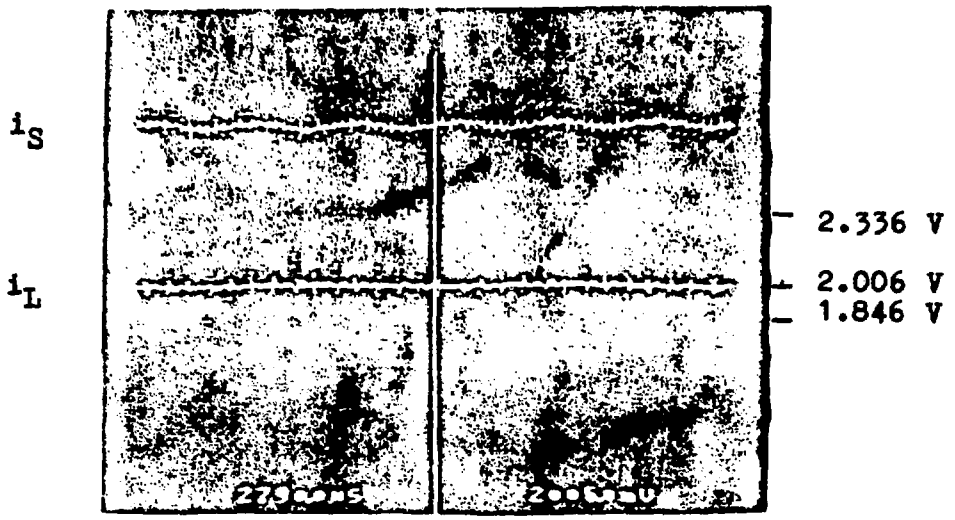

Fig. 4.4. Waveform of the output signal from the DCCT.

resolution of the microcomputer. Each digit approximately corresponds to 2 A. When the ramp signal rises with 15 A/sec, the number of the voltage oscillations is calculated as 7 to 8 in a second. This calculation is verified by the experiment shown in Fig. 4.3.

Figure 4.5 shows the voltage across the thyristor at the instant of switching. The phase difference is changed from - 90° to + 90°. The voltage across each thyristor is increased during the transient period where the dc voltage swings from one extreme to the other. Figure 4.6 shows the capacitor voltage waveform during the shift of the phase difference from 90° to 0° where the current ratio I_S/I_L is 1. In a steady state, the highest switching voltage appears when the phase difference is 0° and the current ratio is 1. During the transient period of the phase shift, the load side converter is only controlled and the waveform of the load side component of the capacitor voltage is expanded. Then the total capacitor voltage is also increased. Therefore, a higher switching voltage can be generated during the transient period than one in a steady state.

The sensitivity of the control system is dependent on the accuracy of the analog instruments and the resolution of the digital devices. In our system, the low resolution of the microcomputer determines the sensitivity. When the sensitivity is increased, the difference between the reference and the feedback signal is decreased with a frequent voltage oscillation. If the voltage oscillation, relevant to this control method, does not deteriorate the system performance, the bang-bang control method is prospective in practice.

5. Modified Open-Loop Control Method

The open-loop control method has been applied to the ICB. The open-loop control method keeps the phase difference and the converter frequency constant during the energy transfer period. The phase difference and the converter frequency are supplied from the external switching board. Then the values, corresponding to the two variables, are loaded in the microcomputer memory and set on the indicators. The process is controlled by the microcomputer command sequence.

The experimental results by the open-loop control method at constant phase difference and frequency show the sinusoidal waveform of the load current during the charge cycle. Also, the magnet current varies smoothly,

Fig. 4.5. Waveform of the voltage across the thyristor (SL4).

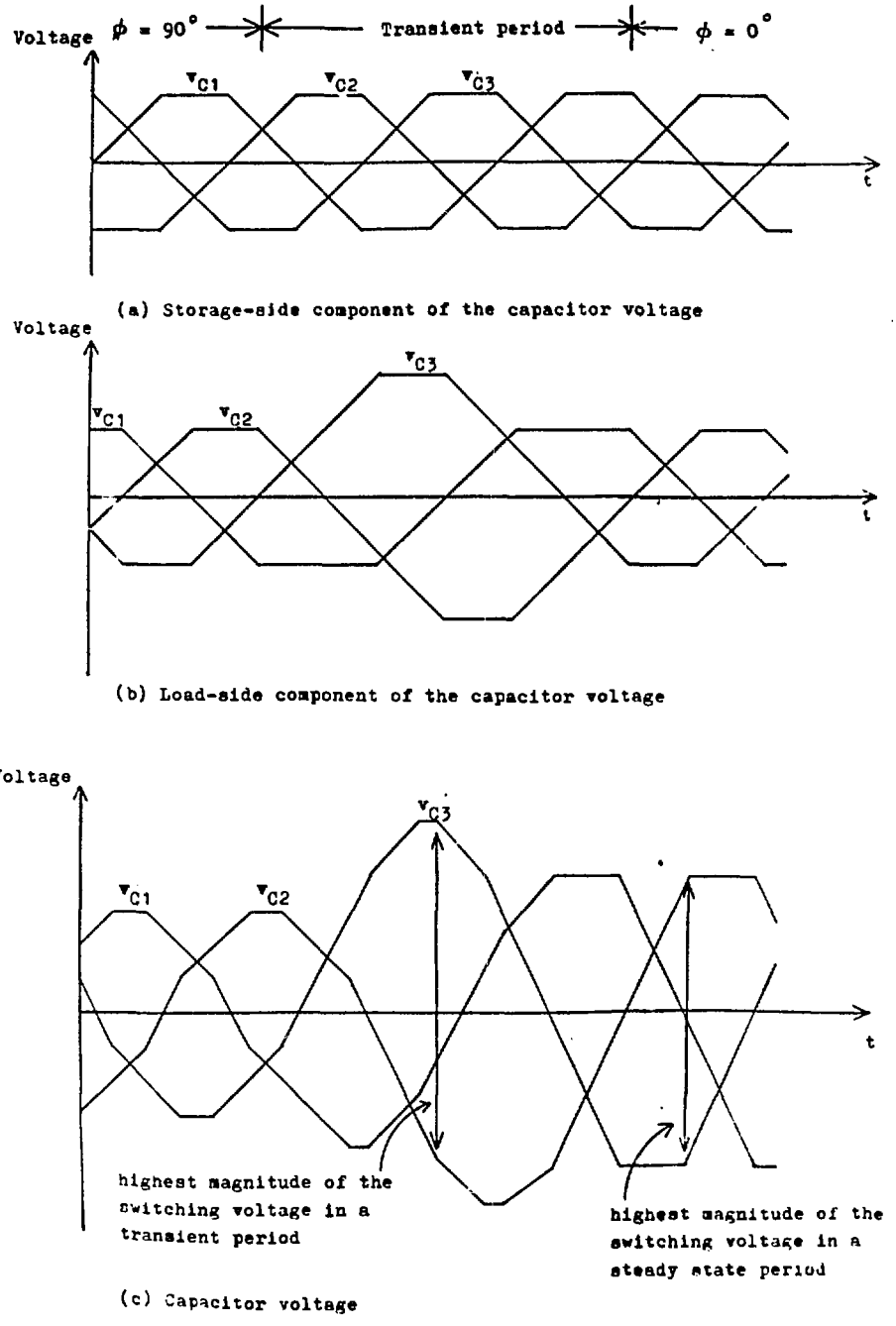

Fig. 4.6. Capacitor voltage waveform during the shift of the phase difference from 90° to 0°, where the current ratio (i_S/i_L) is equal to 1.

although the instantaneous magnet voltage has a discontinuity due to the thyristor switching. The large magnet inductance smooths the magnitude of the noise generated by the thyristor switching so that noises on the two magnet currents are easily eliminated by the low pass filters. A simulation of the open-loop control method in which the energy loss is neglected provides the sinusoidal waveform of the load current. This waveform corresponds to the experimental result. But the sinusoidal waveform of the load current may not be the desired type of the output pattern. A constant current ramp is another applicable type of the output waveform for the ICB.

The open-loop control method, which provides the constant phase difference and converter frequency, is not flexible in its output waveform. It may be desirable to employ the open-loop control method which produces the constant current rise. By using the dynamic equations, the modified open-loop control method is discussed here.

If loss is negligible, the dynamic equations are

$$\frac{di_S(t)}{dt} = -\frac{54\ t_{sw}\ \sin\ \phi}{\pi^3 L_S C}\ i_L(t)\ , \tag{5.1}$$

$$\frac{di_L(t)}{dt} = \frac{54\ t_{sw}\ \sin\ \phi}{\pi^3 L_L C}\ i_S(t)\ , \tag{5.2}$$

where $i_S(t)$ and $i_L(t)$ are the instantaneous storage and load currents, respectively, ϕ is the phase difference, and t_{sw} is the switching interval.

When the rate of the current rise is held constant, the phase difference is expressed as a function of the storage current:

$$\phi = \sin^{-1}\left[\frac{\pi^3 L_L C}{54\ t_{sw}}\quad \frac{di_L}{dt}\quad \frac{1}{i_S(t)}\right], \tag{5.3}$$

where the rate of rise of the load current is constant. Eq. 5.3 is not a suitable function for the microcomputer computation because of its computational complexity and required long execution time. In practice, the phase difference corresponding to the storage current for the given rate of the

current rise is precalculated and loaded in the consecutive microcomputer memory locations. Then the storage current is measured by the DCCT and converted into the digital signal by the A/D converter. The microcomputer determines the phase difference by searching the contents of the memory corresponding to the value of the detected storage current.

When the loss due to the thyristor forward voltage drop is added in Eq. 5.2, the equation becomes

$$\frac{di_L(t)}{dt} = \frac{54\ t_{sw}\ \sin\phi}{\pi^3 C}\ \frac{1}{L_L}\ i_S(t) - \frac{2V_f}{L_L}\ . \tag{5.4}$$

For the given rate of the current rise and the thyristor forward voltage drop, the phase difference is expressed as follows:

$$\phi = \sin^{-1}\left[\ \frac{\pi^3 C L_L}{54\ t_{sw}}\ \left(\frac{di_L}{dt} + \frac{2V_f}{L_L}\right)\ \frac{1}{i_S(t)}\ \right]. \tag{5.5}$$

The coefficient of the inverse of the storage current is slightly increased in Eq. 5.5 compared with one in Eq. 5.3.

During the constant current period, the storage unit only delivers enough energy to compensate for the energy loss. The dynamic equation, including the energy loss due to the wiring resistance and to the thyristor forward voltage drop, is expressed as follows:

$$\frac{di_L(t)}{dt} = \frac{54\ t_{sw}\ \sin\phi}{\pi^3 L_L C}\ i_S(t) - \frac{R_L}{L_L}\ i_L(t) - \frac{2V_f}{L_L}\ . \tag{5.6}$$

From the zero rate of the current rise and the constant load current, the phase difference is expressed as follows:

$$\phi = \sin^{-1}\left[\ \frac{\pi^3 L_L C}{54\ t_{sw}}\ \left(\frac{R_L}{L_L}\ I_L^o + \frac{2V_f}{L_L}\right)\ \frac{1}{i_S(t)}\ \right], \tag{5.7}$$

where I_L^o is the assigned constant value of the load current. The phase difference is a function of the storage current similar to the form for the period of constant current rise. However, the coefficient of the inverse of the storage current in Eq. 5.7 is small because of the low wiring resistance and thyristor forward voltage drop. Therefore, the phase difference remains at a small positive value until the end of the energy transfer period.

In order to apply Eq. 5.7 for the control of the load current, we need a precise expression of the energy loss. The wiring resistance and the thyristor forward voltage drop have been measured in an experiment. The simulated result, obtained by the dynamic equations with the measured parameters, does not exactly agree with the experimental results. (See Section 7.) Perhaps the thyristor switching loss may not be negligible compared with the loss due to the wiring resistance and to the thyristor forward voltage. So far, the coefficients of the two loss terms are modified in order to reduce the difference between the simulated and the experimental results. Therefore, Eq. 5.7 may not provide the exact phase difference necessary for the compensation of the energy loss.

The experimental results by the open-loop control method compared with ones by the modified open-loop control method are shown in Figs. 5.1(a) and 5.2(a). The phase difference in each figure is determined in such a way that it provides the same rate of rise of the load current as the experimental result by the modified open-loop control method does at the beginning of the energy transfer period. The following characteristics of the open-loop control method are obtained from the experimental results: (1) The load current varies sinusoidally and its rate of rise is gradually decreased. (2) When the phase difference is increased or the converter frequency is decreased, the energy transfer rate is increased.

The phase difference and the converter frequency are shown in each figure. The time of the energy transfer period is 6.12 and 7.56 sec in Figs. 5.1(a) and 5.2(a), respectively. Even though the phase difference in Fig. 5.2(a) is greater than the one in Fig. 5.1(a), the time of the energy transfer period is decreased in Fig. 5.1(a) because of the low converter frequency. In both cases, about 72% of the total energy, corresponding to the load current of 85 A, is delivered from the storage to the load units.

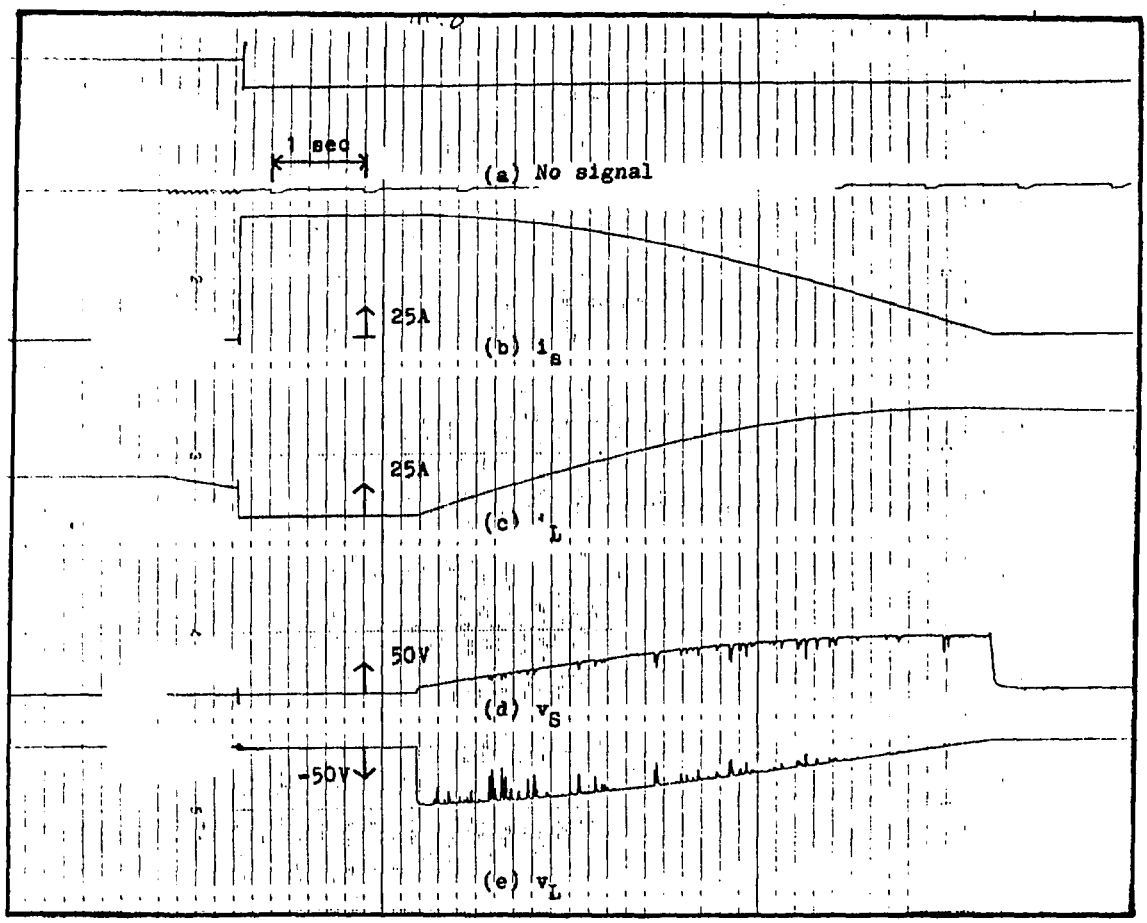

Fig. 5.1. Comparison between the open-loop and the modified open-loop control methods, where the initial rate of rise of the load current is 25 A/sec.

(a) Experimental result by the open-loop control method where $\phi = 30°$ and $f = 631$ Hz.

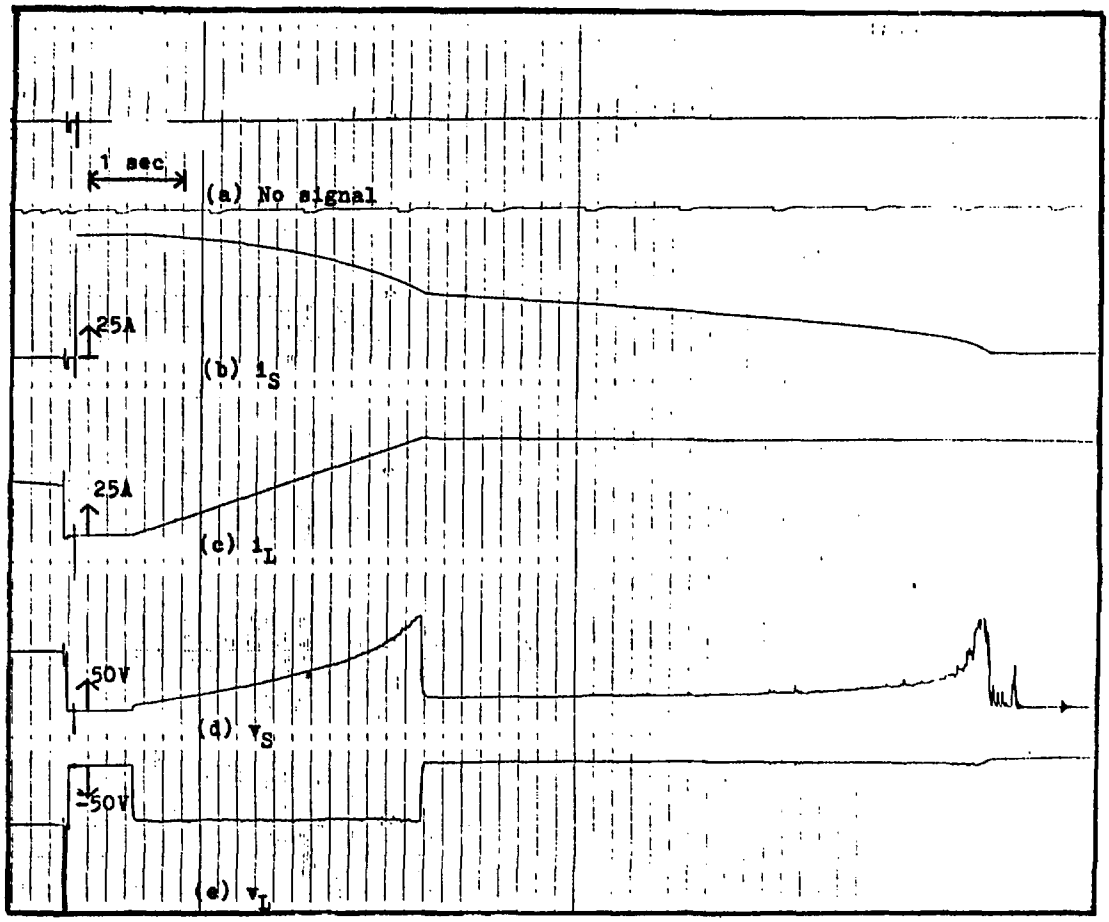

Fig. 5.1. Comparison between the open-loop and the modified open-loop control methods, where the initial rate of rise of the load current is 25 A/sec.

(b) Experimental result by the modified open-loop control method, where $\frac{di_L}{dt}$ = 25 A/sec, f = 631 Hz, and i_{STOP} = 75 A.

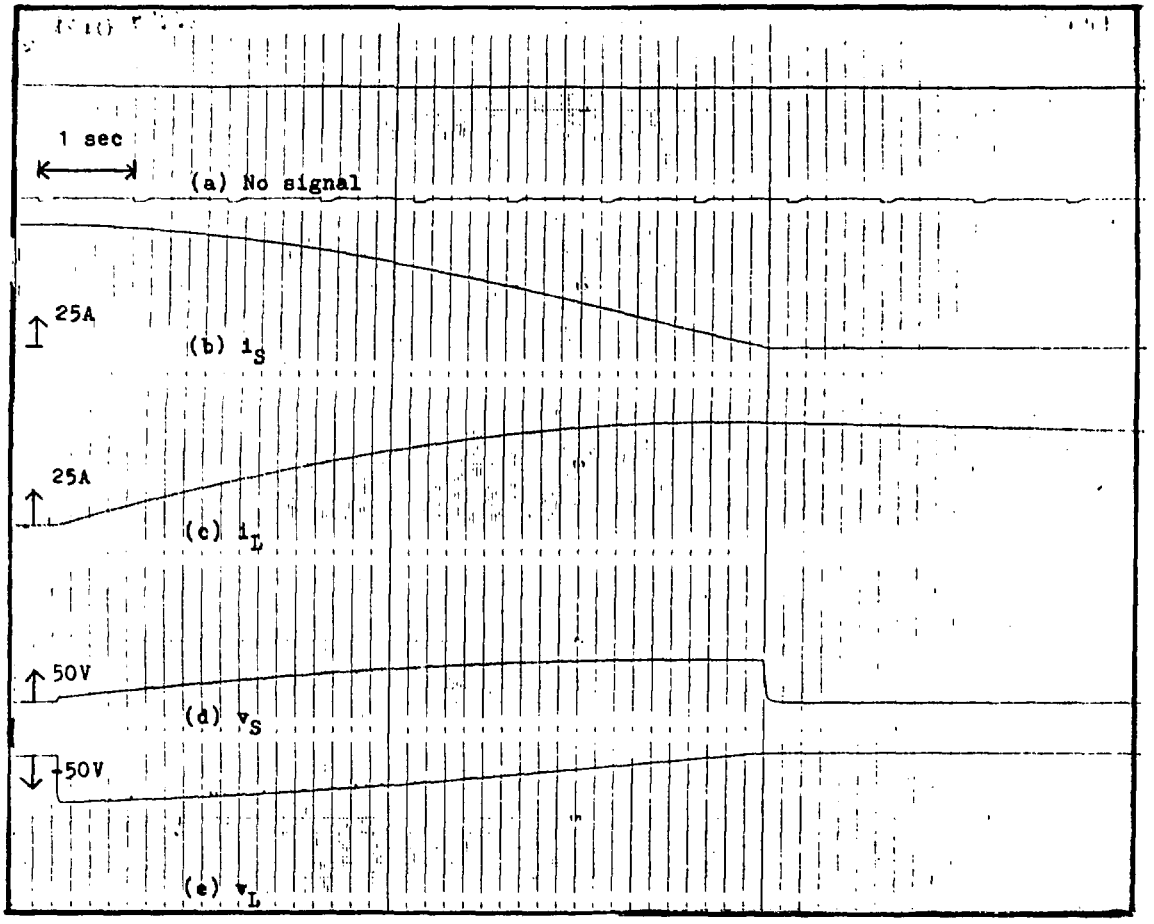

Fig. 5.2. Comparison between the open-loop and the modified open-loop control methods, where the initial rate of rise of the load current is 20 A/sec.

(a) Experimental result by the open-loop control method, where $\phi = 48°$ and $f = 1157$ Hz.

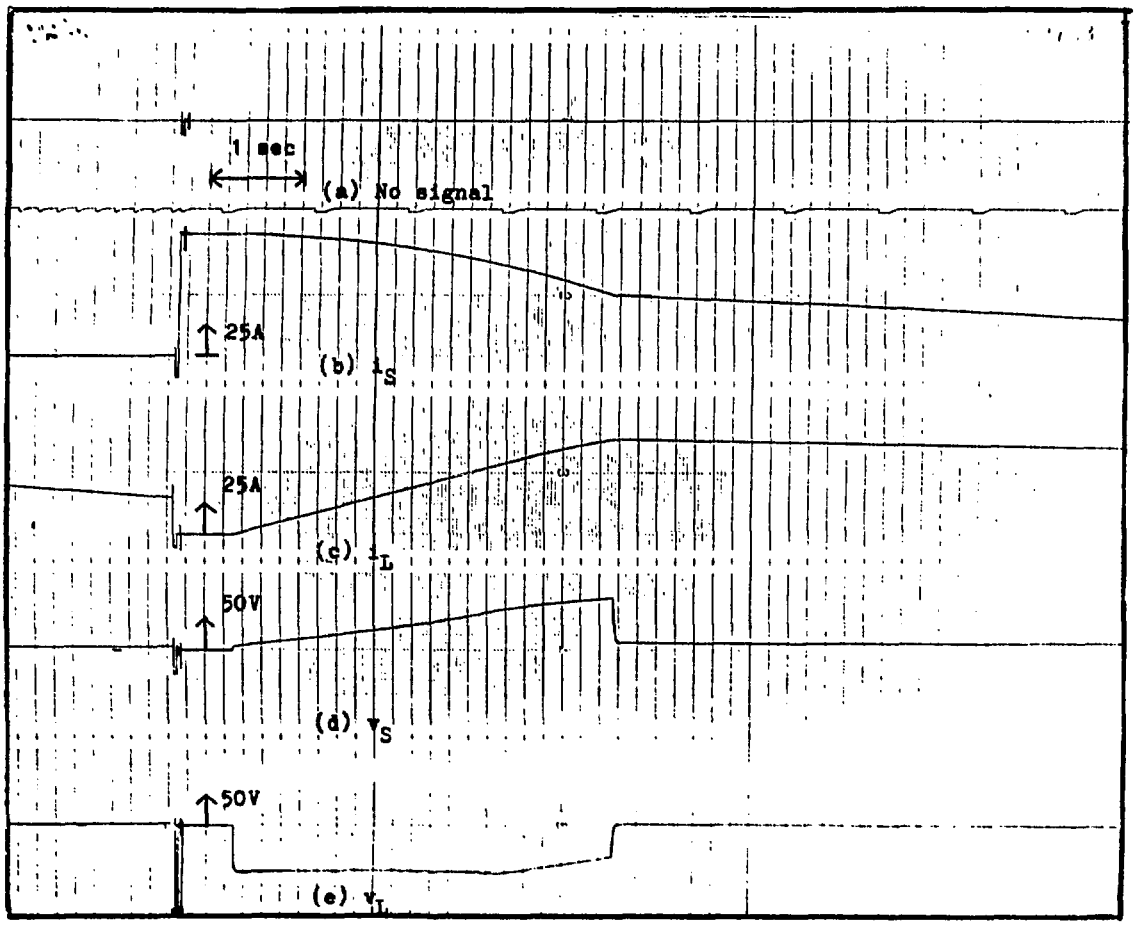

Fig. 5.2. Comparison between the open-loop and the modified open-loop control methods, where the initial rate of rise of the load current is 20 A/sec.

(b) Experimental result by the modified open-loop control method, where $\frac{di_L}{dt}$ = 20 A/sec, f = 1157 Hz, and i_{STOP} = 75 A.

The ripples on the two dc voltages, observed especially in Fig. 5.1(a), appear in both sides at the same time. They do not seem to be random noises picked up by the individual measurement device because of their concurrence. Commutation failure may be one of the possible causes. However, the unbalance of the capacitor voltage, that is a possible result due to the commutation failure, has not been observed. So far, this problem has been deferred.

In order to obtain the list of phase differences corresponding to the storage currents for the modified open-loop control method, we need the rate of the current rise, the converter frequency, and the holding current. The parameters in each experiment are shown in each figure. The experimental results show 25.16 and 20 A/sec in Figs. 5.1(b) and 5.2(b), respectively. There is a good agreement between the parameter used in the calculation and the experimental result. The load voltage, proportional to the rate of the current rise, remains constant as far as the phase difference is controllable. Figure 5.2(b) shows the droop of the load voltage after the load current reaches about 55 A. The phase difference reaches the maximum, 90°, at this time and holds its value. Then the rate of rise of the load current is lowered and the load voltage is decreased.

During the constant current period, the load current cannot hold its assigned value, but the storage voltage is increased as shown in Fig. 5.1(b). Therefore, the modified open-loop control method seems to be working. However, it does not provide enough energy transfer to compensate for the energy loss. The values of the wiring resistance and the thyristor forward voltage drop have to be carefully examined. In addition, a good mathematical expression for the thyristor switching loss in terms of the storage and the load currents may be necessary.

For the modified open-loop control, the phase difference is determined from the storage current, and it regulates the rate of rise of the load current. The load current is not fed back to the microcomputer for the control computation. But the storage current is internally related to the load current so that the use of the storage current in the control algorithm may form the feedback control system. Fortunately, we have not observed the possible current or voltage oscillation which may be the characteristics of the linear feedback control system.

Figures 5.3(a) and 5.3(b) show the experimental results by the bang-bang control method and by the modified open-loop control method, respectively, for the same converter frequency and rate of the current rise. In Fig. 5.3(a), the load current oscillates in a small range, determined by the quantization band. However, the rate of rise of the load current approximately remains constant. The load and storage current waveforms in Figs. 5.3(a) and 5.3(b) have a good agreement. On the other hand, the two voltage waveforms in Figs. 5.3(a) and 5.3(b) are quite different from each other. The bang-bang control method produces the voltage oscillation with the high magnitude. But its average waveform should be equal to the one shown in Fig. 5.3(b). The envelope of the load voltage covers the range of + 105 and - 105 V, while its average remains about 55 V as far as the load current is controllable.

In Fig. 5.3(a), the final voltage oscillation, shown as a small depression, takes place at the load current of about 70 A. In Fig. 5.3(b), the droop of the load voltage starts at the same current value. After this moment, the phase difference holds its maximum. But it cannot hold the constant rate of the current rise and the load voltage starts to droop. Then, the dc voltages in Figs. 5.3(a) and 5.3(b) are varied in the same way.

6. Frequency Modulation Method

The phase difference and the converter frequency are the controllable parameters for the ICB. The phase difference modulation provides the control of the energy transfer direction and its rate. The phase difference is altered by increasing the switching interval produced at one of the two pulse sequencers. The side at which the pulse sequencer is controlled depends on whether the phase difference advances or retards. On the other hand, the frequency modulation provides the control of the energy transfer rate but not its direction. The converter frequency is altered by increasing or decreasing the switching interval produced at the two pulse sequencers. The frequency shift will alter the relative relationships of the phase difference.[9] In order to correct the phase difference, the phase shift must be induced along with the frequency shift. The hardware and software are more complicated for the frequency modulation case. However, controllability of the converter frequency as well as the phase difference is one of the characteristics of the ICB. It is also conceivable to combine the two modulation

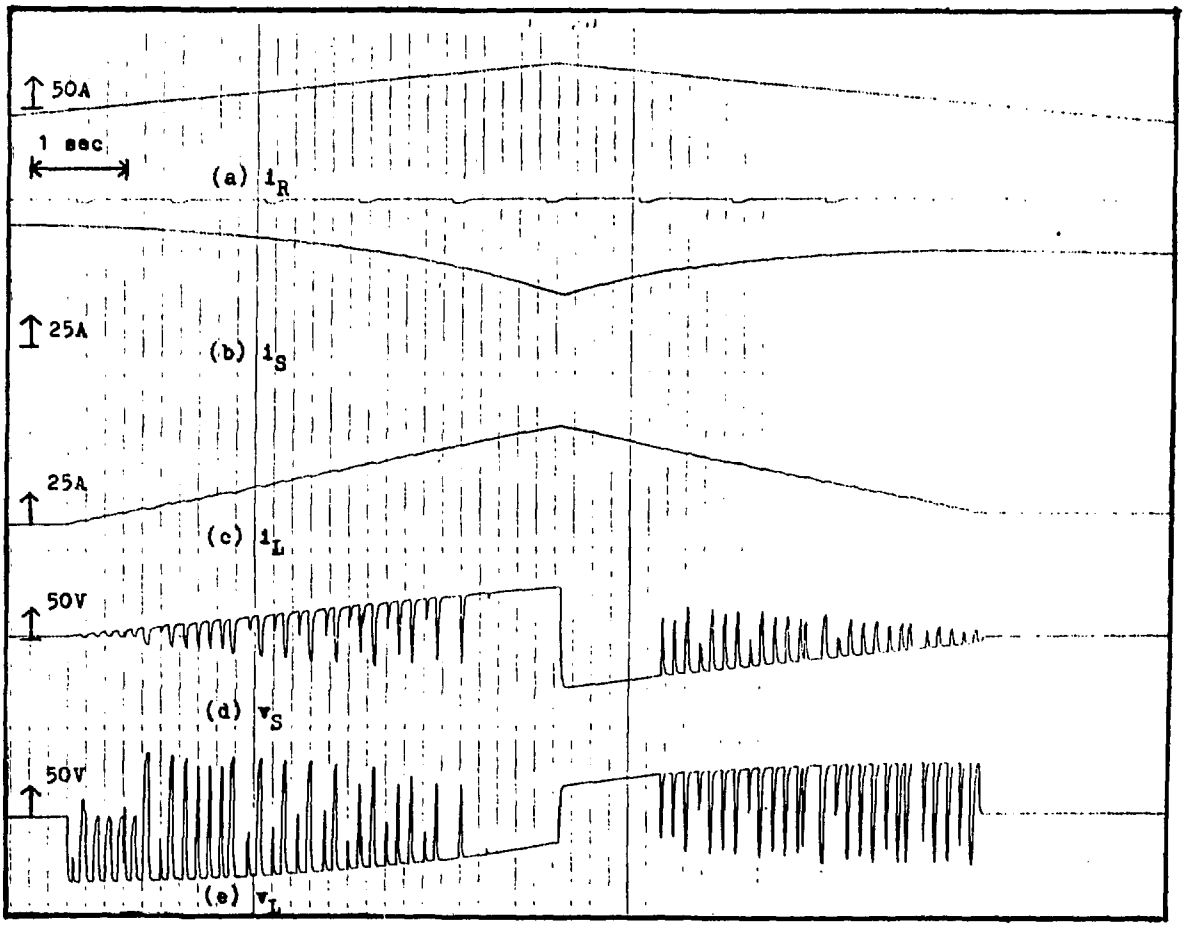

Fig. 5.3. Comparison between the bang-bang and modified open-loop control methods.

(a) Experimental result by the bang-bang control method, where $\frac{di_L}{dt}$ = 15 A/sec and f = 1157 Hz.

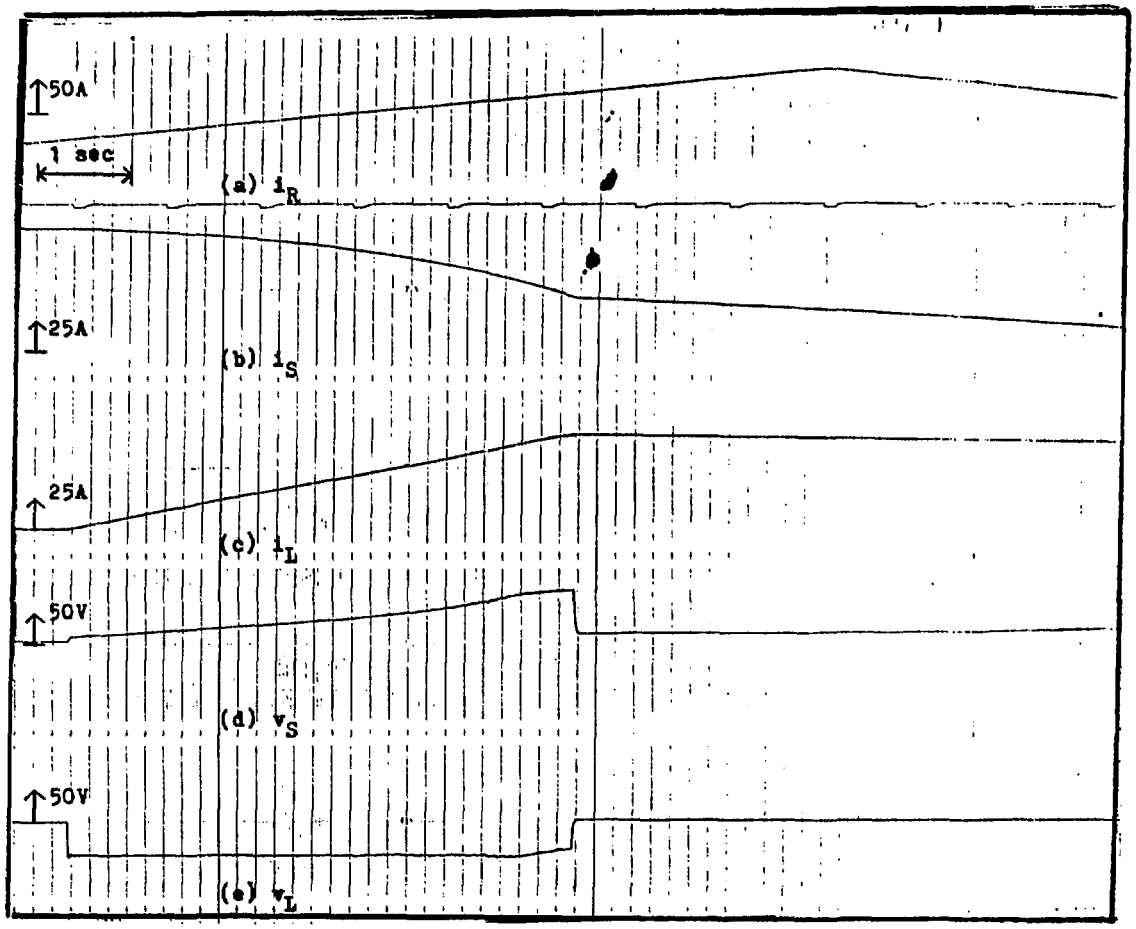

Fig. 5.3. Comparison between the bang-bang and modified open-loop control methods.

(b) Experimental result by the modified open-loop control method, where $\frac{di_L}{dt}$ = 15 A/sec, f = 1157 Hz, and i_{STOP} = 75 A.

methods for fine control of the energy transfer process. Kustom and Fuja have accomplished a technique on the phase difference modulation and its implementation.[2] Barnard and Kustom have also developed a technique on the frequency modulation.[14]

The present pulse sequencers can provide the frequency as well as the phase difference modulation but do not precisely accept the frequency modulation method introduced here. At first, we explain the phase and the frequency shifting techniques and describe the performance of the present pulse sequencers. Then we discuss the difficulties of the frequency modulation due to the method itself and to the limitation of the present hardware. The experimental result by the feedback control method with frequency modulation is shown at the end of this chapter.

The phase and the frequency shifting techniques can be described by the sequence of the switching interval during transients in the matrix form. The phase shifting technique takes place in four steps. The subscripts, S and L, correspond to the storage and the load side. After the transient steps, the switching interval remains constant. The transient sequence, $S_{S\ (or\ L)}$, in the matrix form is expressed as follows:

$$S_{S\ (or\ L)} = \begin{bmatrix} \Delta t_{1S\ (or\ L)} \\ \Delta t_{2S\ (or\ L)} \\ \Delta t_{3S\ (or\ L)} \\ \Delta t_{4S\ (or\ L)} \end{bmatrix} = \begin{bmatrix} 1 & 1 \\ 1 & 0 \\ 1 & 0 \\ 1 & 1 \end{bmatrix} \begin{bmatrix} \Delta t_0 \\ \Delta t_1 \end{bmatrix}, \qquad (6.1)$$

where Δt_{iS} and Δt_{iL} are the i-th interval of a four-step switching transient on the storage and load converters, respectively; Δt_0 is the switching interval before transients; and Δt_1 is the increment assigned to execute half of the desired phase shift.

The converter frequency of the ICB is altered by increasing or decreasing the switching intervals at both converters. It can be shown that both converters must operate at the same frequency. The simplest way to change the operating frequency and still maintain the balanced phase voltage is a three-step frequency shifting technique. After the transient sequence, the switching interval, $\Delta t_0'$, is $\Delta t_0 + \Delta t_2$. The transient sequences, S_S and S_L, are expressed as follows:

$$S_S = \begin{bmatrix} \Delta t_{1S} \\ \Delta t_{2S} \\ \Delta t_{3S} \end{bmatrix} = \begin{bmatrix} 1 & 1 \\ 1 & 0 \\ 1 & 1 \end{bmatrix} \begin{bmatrix} \Delta t_0 \\ \Delta t_2 \end{bmatrix}, \tag{6.2}$$

$$S_L = \begin{bmatrix} \Delta t_{1L} \\ \Delta t_{2L} \\ \Delta t_{3L} \end{bmatrix} = \begin{bmatrix} 1 & 1 \\ 1 & 0 \\ 1 & 1 \end{bmatrix} \begin{bmatrix} \Delta t_0 \\ \Delta t_2 \end{bmatrix}, \tag{6.3}$$

where Δt_{iS} and Δt_{iL} are the i-th interval of a three-step transient sequence at the storage and the load converters, respectively; Δt_0 is the switching interval before the transient sequence; and Δt_2 is the increment to cause the desired frequency shift.

Figure 6.1 shows the block diagram of the pulse sequencers. The 8-bit down counter and the distributer generate the trigger pulse sequences and deliver them to both converters. The two 8-bit down counters are driven by the output pulses of the 4-bit down counter. The fundamental clock frequency is 5 MHz. The digits in the 4-bit down counter are determined by the rotary switch on the external board. The 8-bit down counter loads the 120 digits as the switching interval of 60° when the output pulse is sent from the 8-bit down counter to its series-connected distributer. The distributer determines which gate is fired and sends the trigger pulse to the thyristor gate and an interrupt signal to the microcomputer at the same time. When the change of the switching interval is not required, the interrupt mask prevents an interrupt signal from halting the microcomputer command sequences.

The converter frequency is altered by changing the digits in the 4-bit down counter. With 120 digits in the 8-bit down counter, the change of the digits in the 4-bit down counter yields the sixteen available converter frequencies, scattered from 400 to 7K Hz. The limited number of the available converter frequencies restricts controllability of the energy transfer rate by frequency modulation. Also, the wide gap between the two adjoining available converter frequencies may cause the thyristor switching to violate the commutation condition.

The alternative method for frequency modulation is to control the base digits of the 8-bit down counter. If the 120 digits is chosen as the switching interval of 60°, each digit of an increment of the switching interval, Δt_1, yields the phase shift of one degree. Therefore, the control

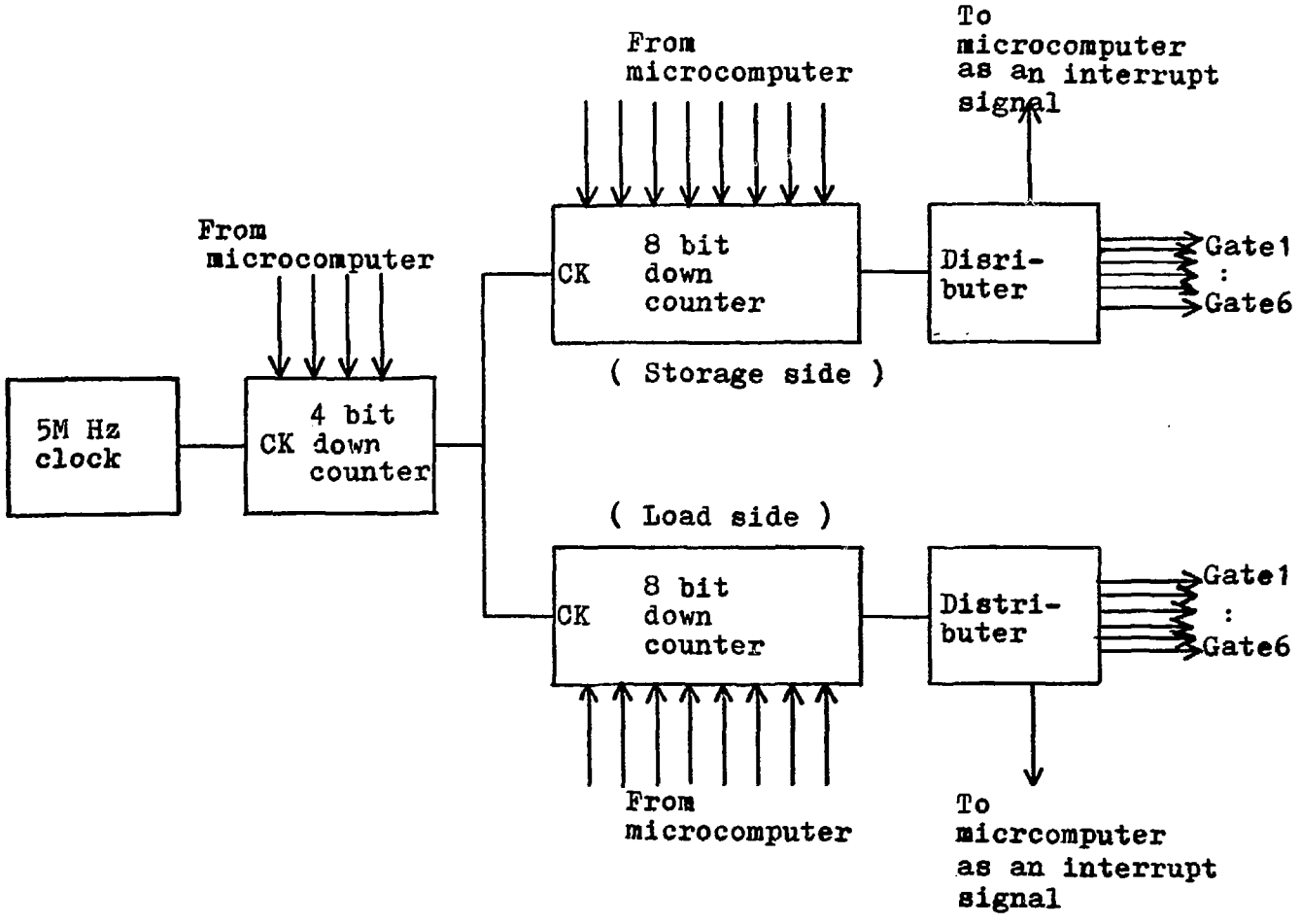

Fig. 6.1. Block diagram of the pulse sequencers.

to 60°, are changed, the increment of the switching interval may become a fractional number, which cannot be acceptable in a digital system. In order to avoid the fractional numbers for increments of the switching interval, the phase difference and the converter frequency are restricted. But this method is the possible method of the frequency modulation for the present hardware.

In order to keep the constant phase difference before and after the frequency shift, the following equation must be satisfied:

$$\frac{\Delta t_{\phi 0}}{t_0} = \frac{\Delta t_{\phi 1}}{t_1} = \frac{\phi}{60} , \tag{6.4}$$

where $\Delta t_{\phi 0}$ and $\Delta t_{\phi 1}$ are the time differences between the gate trigger pulses to the thyristors with the same number at both converters before and after the frequency shift, respectively; t_0 and t_1 are the switching intervals before and after the frequency shift, respectively; and ϕ is the constant phase difference before and after the frequency shift.

The phase shift $\Delta(\Delta t_\phi)$ after the frequency shift is expressed as follows:

$$\Delta(\Delta t_\phi) = \Delta t_{\phi 1} - \Delta t_{\phi 0} . \tag{6.5}$$

The switching intervals before and after the transient and the phase shift after the transient must be products of the integer and the clock cycle of the 8-bit down counter such that

$$\begin{aligned} t_0 &= Iu, \\ t_1 &= Ju, \\ \Delta(\Delta t_\phi) &= Ku, \end{aligned} \tag{6.6}$$

where I, J, and K are integers, and u is the clock cycle of the 8-bit down counter. Substituting Eq. 6.4 into Eq. 6.5 yields

$$\Delta(\Delta t_\phi) = \frac{\phi}{60} (t_1 - t_0) , \tag{6.7}$$

and the further substitution of Eq. 6.6 into Eq. 6.7 gives us

$$Ku = \frac{\phi}{60} (Ju - Iu) ,$$

or

$$\frac{J - I}{K} = \frac{60}{\phi} \quad . \tag{6.8}$$

Equation 6.8 provides the available switching intervals for the pulse sequencers. For example, a 40-degree phase difference provides the following equation:

$$\frac{J - I}{K} = \frac{3}{2} \quad . \tag{6.9}$$

The phase must be shifted by two digits after every three-digit change of the switching interval in order to keep the phase difference constant.

With the control of the digits in the 8-bit down counter, the switching interval sequences are changed at the two pulse sequencers. But their control takes place at the one after the other pulse sequencers. This transient period provides an additional phase shift.

Figure 6.2 shows the frequency modulation performance of present pulse sequencers. Figures 6.2(a) and 6.2(b) show the waveforms of the capacitor voltage components generated by the switching sequences at the storage and the load converters, respectively. The phase differences before transients is equal to zero. Therefore, the phase shift is not necessary if zero degrees of phase difference is required after transients. At first, the switching interval is changed at the storage converter and its transient period is shown in Fig. 6.2(a). During this period, the switching interval on the load converter remains constant. Once the frequency shift is completed at the storage converter, the switching interval starts to be changed at the load converter and its period is shown in Fig. 6.2(b). After two transient periods, the switching intervals at both converters are changed to the desired values, but the load side switching sequence leads the storage side by the phase difference, $\Delta\phi$. The additional phase shift is dependent on the phase difference and the converter frequency before and after transients. Therefore, it cannot be easily corrected by simple techniques. It is noted that an increase or a decrease of the additional phase shift after the frequency shift is dependent on which pulse sequencer is controlled first. The additional phase shift is increased when the switching intervals are regulated by the control of the two pulse sequencers in the storage and then in the load side. The decrease of

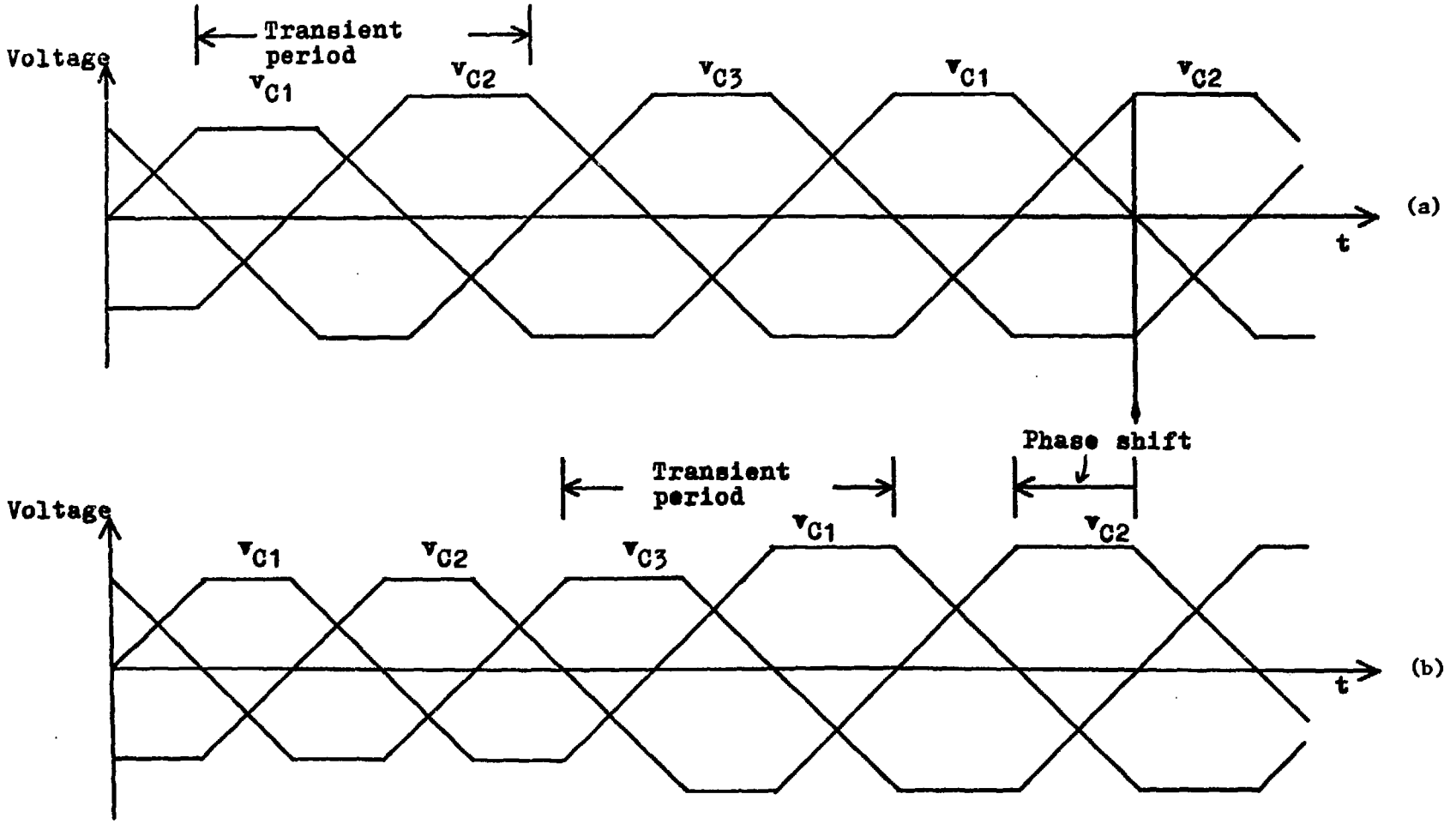

Fig. 6.2. Waveform of the two components of the capacitor voltage during the frequency shift.

(a) Storage side component of the capacitor voltage. (b) Load-side component of the capacitor voltage.

the phase difference is obtained by the control of the two pulse sequencers in the opposite order.

The energy transfer can be controlled by the feedback control method with frequency modulation regardless of the unavoidable change of the phase difference as long as the commutation condition is satisfied. In order to develop adequate frequency modulation in the future, the method of changing the base digits in the 8-bit down counter will be applied to the present experimental system.

Figure 6.3 shows the experimental results for the feedback control method with frequency modulation, where the feedback signal corresponds to the load current. The reference signal, not shown here, rises with the rate of 15 A/sec. The phase shift after the frequency shift is applied for adjustment of theoretically predicted phase relation. The positive error signal introduces an increment of the switching interval and the control of the two pulse sequencers in the storage side and then in the load side. The negative error signal introduces a decrement and the control of the two pulse sequencers in the opposite order. The amount of change in the switching interval is proportional to the error signal within maximum and minimum values. For safety, the initial storage current is charged up to 50 A.

When the reference signal goes through zero voltage, the energy transfer starts from the storage to the load unit. The experimental result shows the rise of the load current with a relatively large magnitude of slow oscillation. It could be due to an instability of the control system, provided by the feedback loop with the linear gain between the error signal and the increment of the switching interval. It could also be due to the control algorithm which did not control the phase angle as the frequency is changed. The two coil voltages oscillate between two extreme voltages determined by the maximum and the minimum converter frequencies and by the phase shift during the transient period of the frequency shift.

While the error signal stays in a controllable region, the digitized error signal does not respond linearly to the change in the real signal but in discrete steps. When the error signal moves from a positive value to negative or vice versa, it passes through zero value and the frequency is kept constant for a while. The time when the error signal stays at zero digit depends on the size of the quantization band (the region where the digital signal cannot

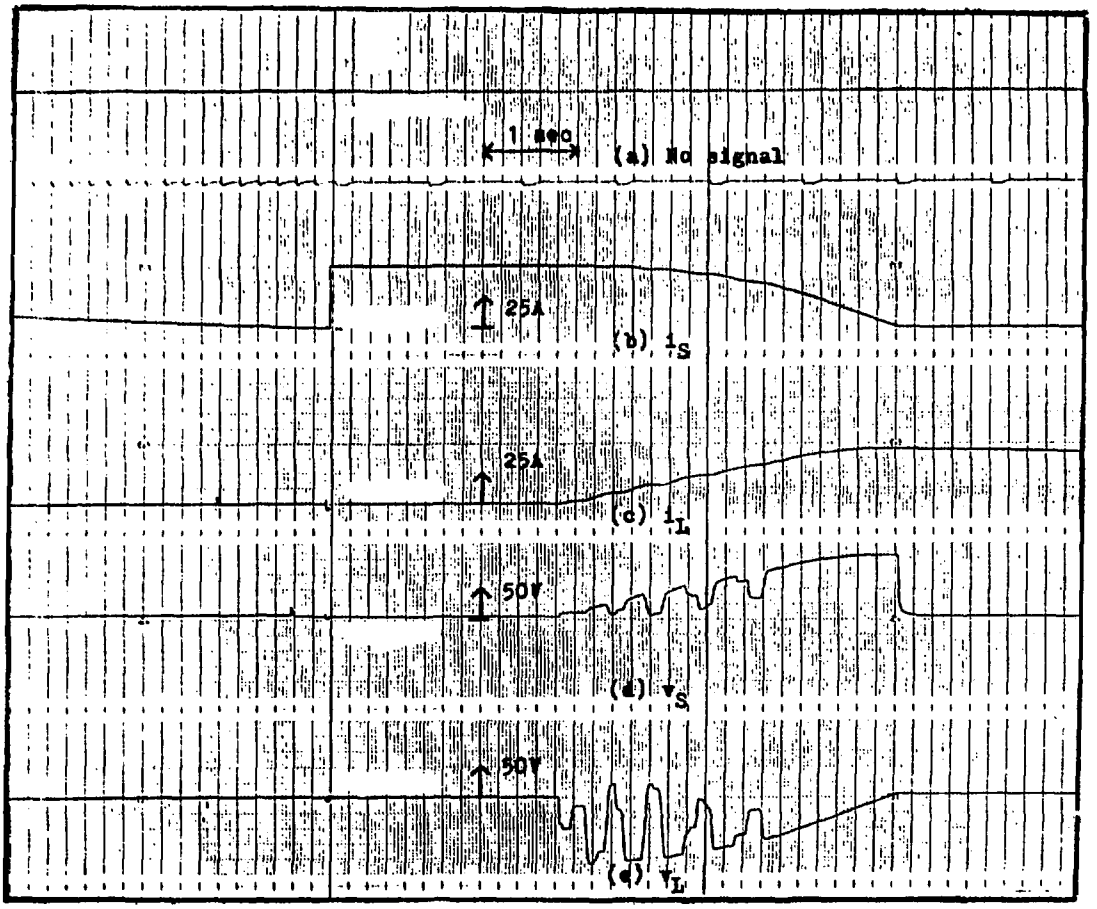

Fig. 6.3. Experimental result by the feedback control method by frequency modulation, where $\phi = 34°$, $f = 1157$ Hz, $f_{min} = 964$ Hz, and $f_{max} = 1446$ Hz.

resolve the change from one real signal to the next). The source of this oscillation will be studied further. At the end of the energy transfer period, the converter frequency is held at its least value because the feedback signal can no longer follow the reference. However, the energy transfer is completed without violation of the commutation condition.

7. Simulation of the Energy Transfer Process

The mutual relation between the storage and the load currents can be described by the dynamic equations, given in Section 3. In order to ensure performance of the control system with the new control algorithm, we need to simulate it with an aid of the large-scale computer. The dynamic equations can be solved by a subroutine from the International Mathematical and Statistical Library (IMSL). The dynamics of the input and the output variables are drawn on the CRT screen by the plotting software package, "TELL-A-GRAF", and printed on the hard copy paper.

The difference between the experimental and the simulated results are characterized by the following:

1. The present simulation program does not take into account the effect of the quantization band, determined by the resolution of the digital device, on the dynamic performance of the control system.

2. According to the sampling theorem,[12] a sampling frequency must be twice greater than the characteristic frequency of the controlled system in order to obtain any necessary information for its control. Hence, a required time step of the computer simulation is lower than half of the minimum switching interval for the phase and the frequency shifts. A small time step requires a large number of iterations and much CPU time to calculate the waveform of the variables for a whole energy transfer period. On the other hand, the dominant time constant may be greater than 570 sec, estimated from the magnet inductance of 4 H and the wiring resistance of 0.007 Ω. Therefore, it is conceivable that the control system does not respond to the change of the input signal within half of the minimum switching interval. The low resolution of the digital

device also causes the slow response of the control system, because the change of the real signal inside a quantization band does not alter the digital signal. The time step is changed with each simulation. A feedback control method requires a smaller time step than does the open-loop control method.

3. In order to satisfy the commutation condition, the phase difference varies between the two extremes, -90° and 90°, while the converter frequency varies within a limited range centered at the initial frequency. However, the dynamic equations do not describe the switching performance during the phase or the frequency shifts. Hence, it must be kept in mind that an abrupt change of the phase difference and the converter frequency may violate the commutation condition in an experiment even though it does not in a simulation.

The measured wiring resistance of 0.007 Ω and thyristor forward voltage drop of 1.2 V produce a smaller amount of the total energy loss in a simulation than that in an experiment. The additional energy loss in an experiment may mainly result from the thyristor switching. In order to reduce the difference in energy loss between an experimental and a simulated result, we adjust the wiring resistance from 0.007 to 0.1 Ω and the thyristor forward voltage drop from 1.2 to 1.5 V in a simulation.

Figure 7.1 shows the load and the storage currents from the simulation, and the load current from the experiment. The phase differences in Figs. 7.1 (a), (b), and (c) are equal to 30°, 60°, and 80°, respectively, while the converter frequency is held at 631 Hz. The phase difference and the converter frequency remain constant during the energy transfer period. In Figs. 7.1(b) and (c), the magnitude of the load current in an experiment is slightly higher than that in a simulation. But the fundamental waveforms of the two currents are well matched. In Fig. 7.1(a), the magnitude of the load current in the simulation is relatively higher than that in an experiment at the end of the energy transfer period, although the two current magnitudes are matched in the first few seconds. The difference between the simulated and the experimental results is large at a low phase difference. The dynamic simulation model satisfactorily describes the experimental results. It is noted that the wiring resistance and the thyristor forward voltage drop may have to be altered for a different converter frequency because the thyristor switching

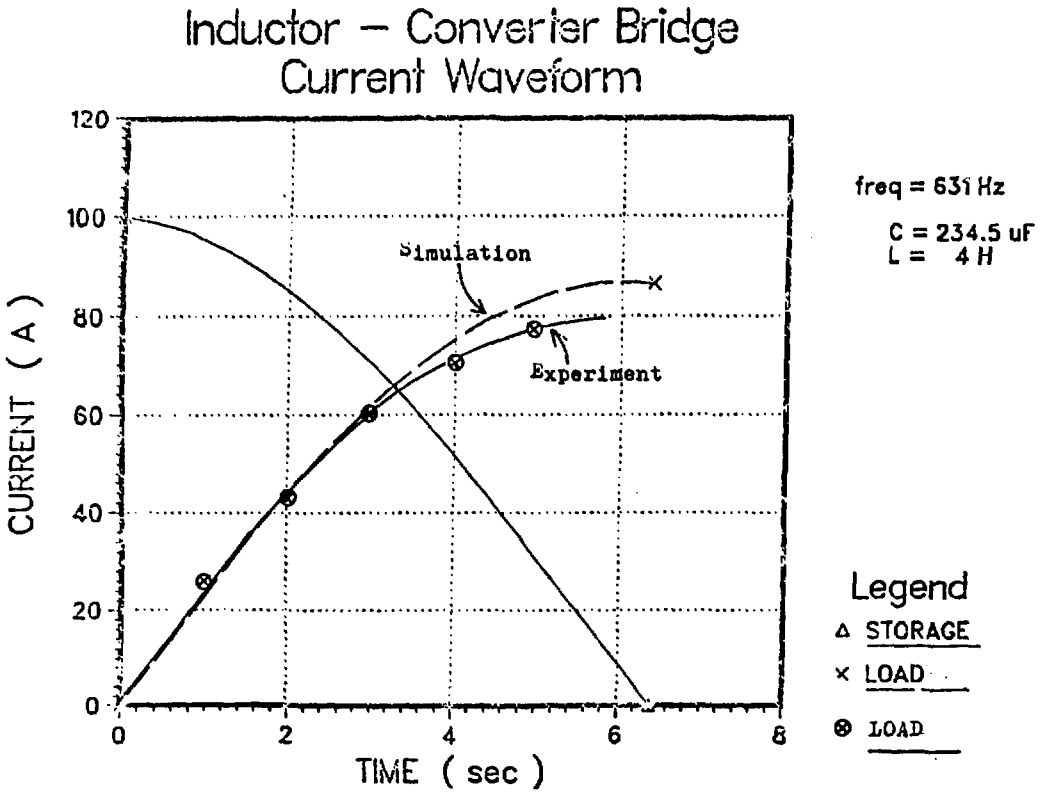

Fig. 7.1. Comparison between the current waveforms of the experiment and of the simulation for adjustment of the energy loss terms ($R_S = R_L = 0.05$, $V_f = 1.5$ V).

(a) $\phi = 30°$

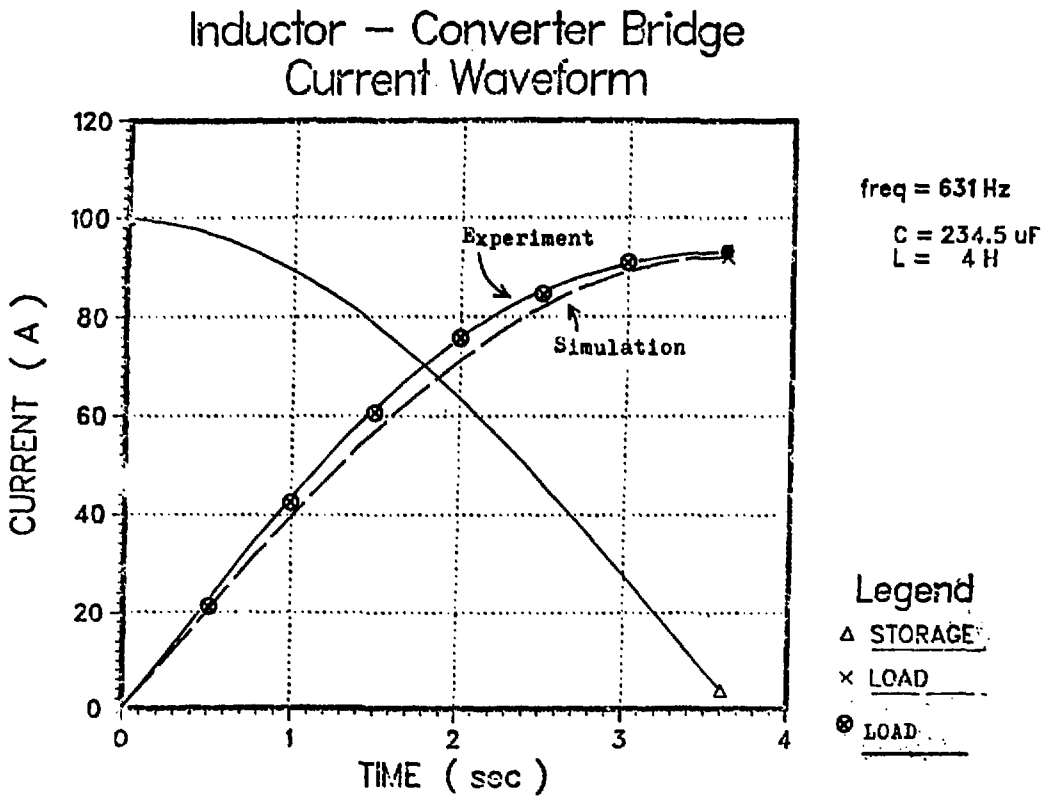

Fig. 7.1. Comparison between the current waveforms of the experiment and of the simulation for adjustment of the energy loss terms ($R_S = R_L = 0.05$, $V_f = 1.5$ V).

(b) $\phi = 60°$

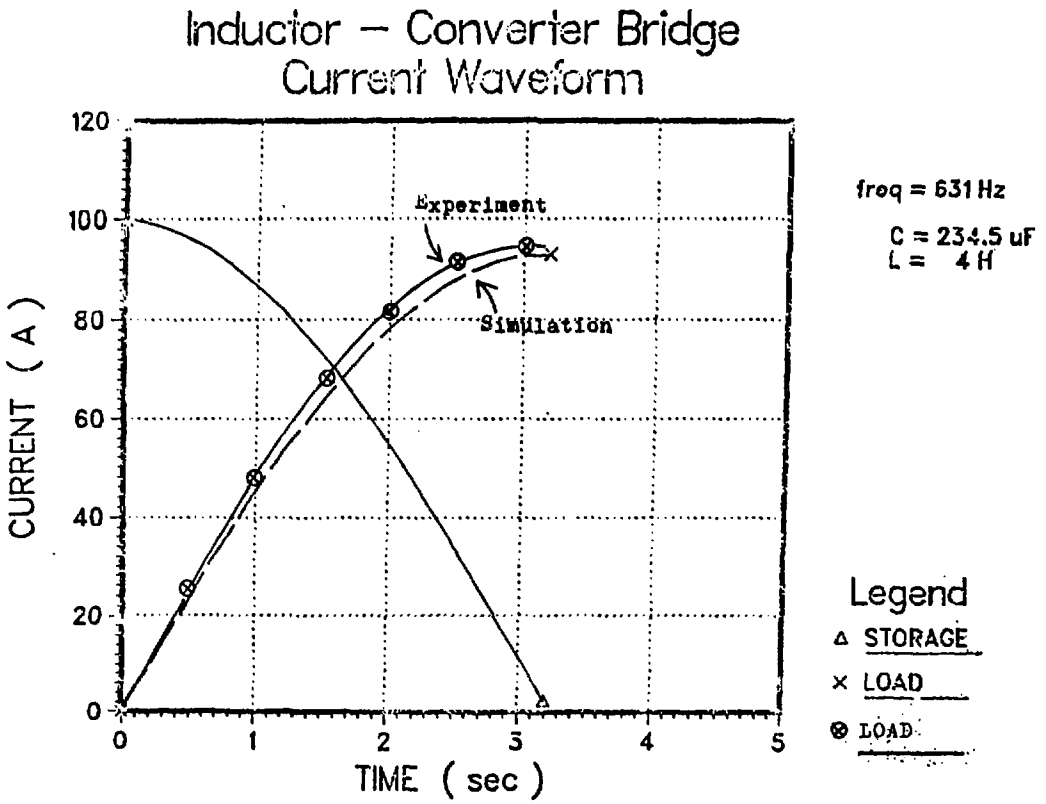

Fig. 7.1. Comparison between the current waveforms of the experiment and of the simulation for adjustment of the energy loss terms ($R_S = R_L = 0.05$, $V_f = 1.5$ V).

(c) $\phi = 80°$

loss is dependent on the number of the thyristor switchings. It is also noted that a large time step may not adequately describe the dynamic performance because of the time-variable coefficients of the dynamic equations.

7.1 Modified Open-Loop Control Method

Figure 7.2 shows the flow chart of the modified open-loop control method. The rate of the current rise and the switching interval are initially specified for calculation of the coefficient of the control equation, that is, the equation derived from the dynamic equations without energy loss. The phase difference is determined from the control equation with the present storage current at each time step. The dynamic equations with the varied phase difference provide the two current values at the next time step. Energy is delivered until the storage current becomes lower than zero.

In order to simulate the system dynamics for a period of constant current as well as for a current rise period, we specify the current value at which we change the mode of the load current. When the load current reaches the given current value, the period of the load current is altered from constant current rise to constant current by the change of the control equation. Then we repeat the procedure described in the flow chart in Fig. 7.2.

Figures 7.3(a) and (b) show the simulated and the experimental results, respectively, by the modified open-loop control method, where the rate of the current rise is 25 A/sec. While the phase difference varies within the two extremes, the load current rises with the constant rate. In Fig. 7.3(a), its rate of rise is slightly lower than the desired one, which is drawn as a straight line from the origin. The difference between the desired and the simulated waveforms may be due to the energy loss which are not considered in the modified open-loop control method. A time step is 0.2 sec.

In Fig. 7.3(b), the load current rises with the rate of 25 A/sec. The modified open-loop control method in the experiment provides a better result than one in a simulation because of the increased capacitance from 200 to 234.5 μF in the control equation. An increased coefficient of the control equation introduces more energy transfer than the expected one. Then the energy transfer supplies enough energy to compensate for the energy loss as well as to keep the desired rate of the current rise. It follows that the adjustment of the coefficient in the control equation provides the desired rate of current rise. The other experimental results by the modified open-

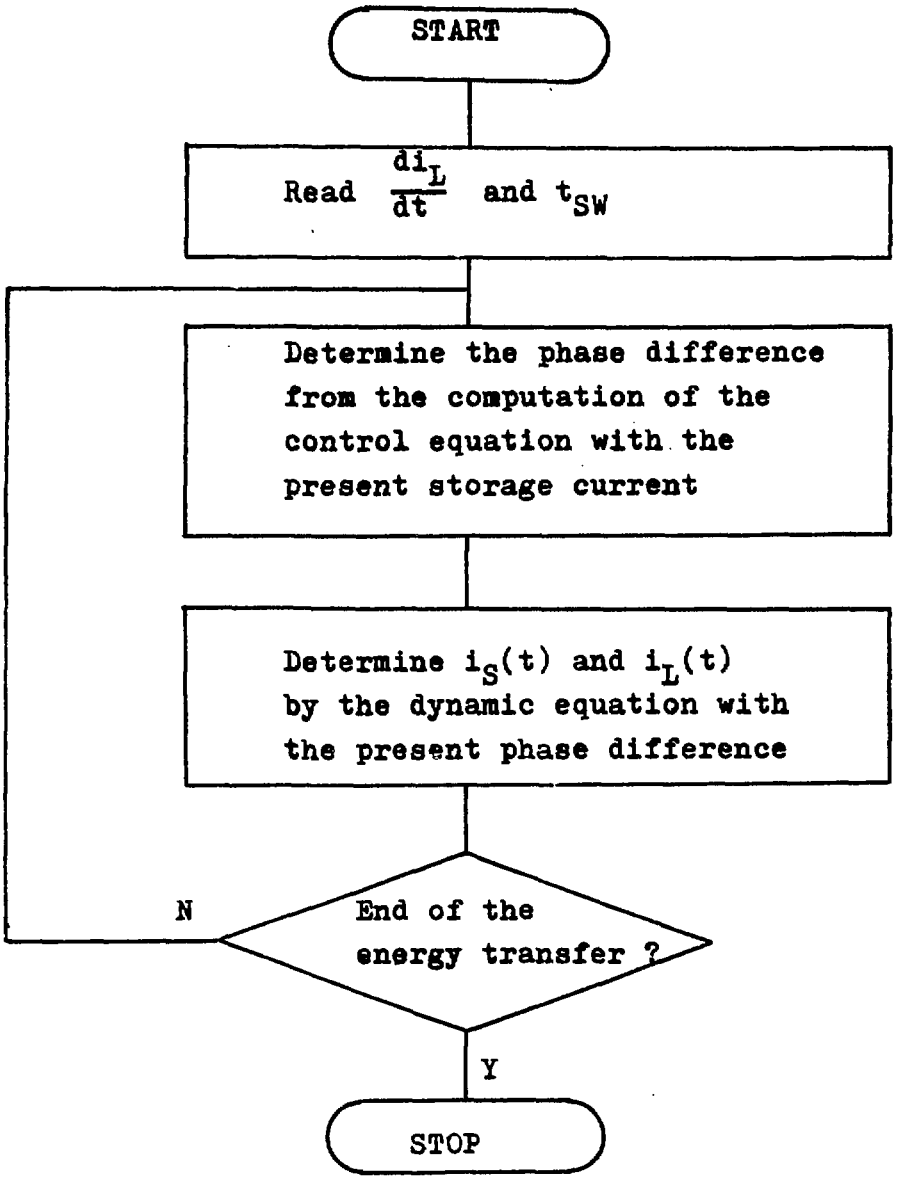

Fig. 7.2. Flowchart of the modified open-loop control method.

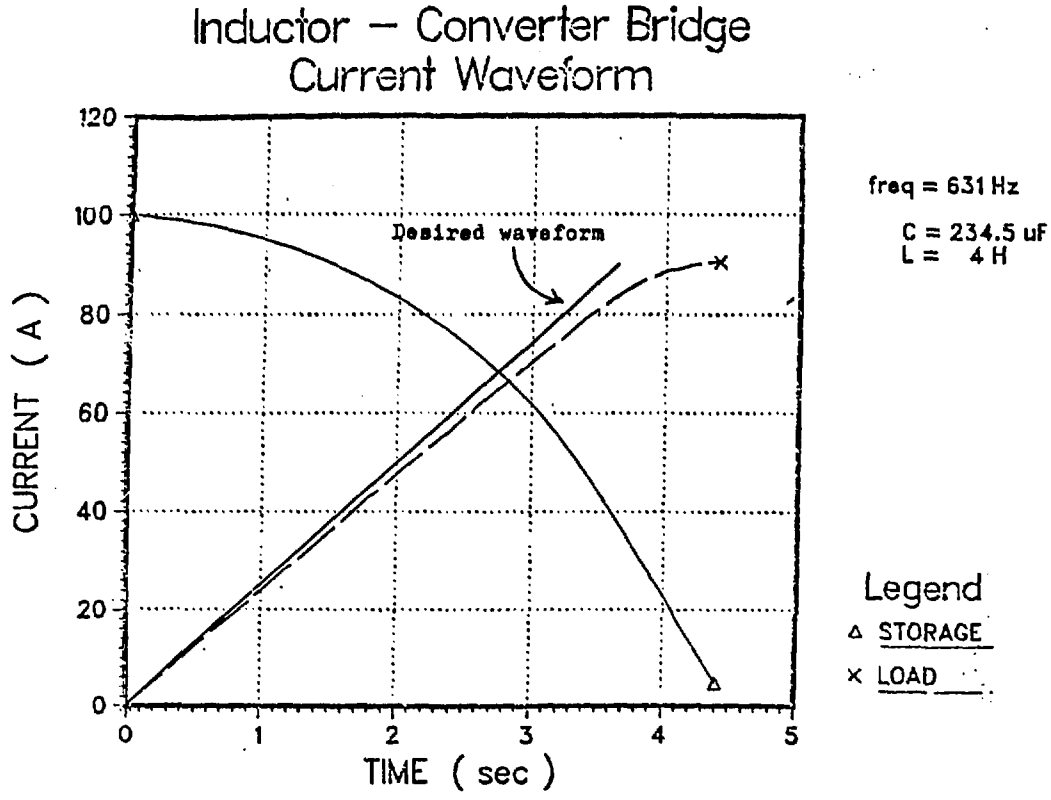

Fig. 7.3. Comparison between the current waveforms regulated by the modified open-loop control method at simulation and at experiment.

(a) Result of the simulation.

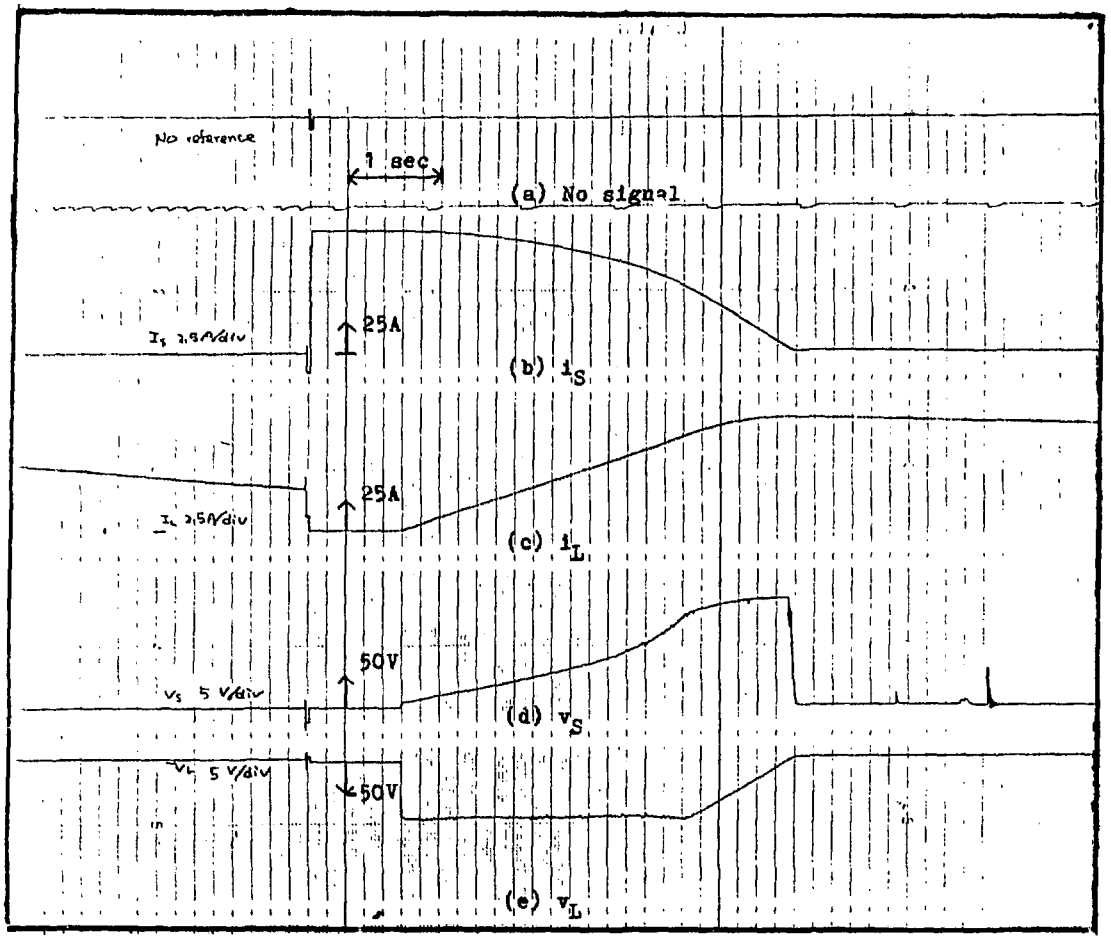

Fig. 7.3. Comparison between the current waveforms regulated by the modified open-loop control method at simulation and at experiment.

(b) Result of the experiment.

loop control method, in Section 5, are also obtained by using the capacitance of 234.5 μF.

7.2 Feedback Control Method by Frequency Modulation

Figure 7.4 shows the flow chart of the feedback control method by frequency modulation. The rate of the current rise and the current value at which we change the mode of the load current is initially specified. The reference signal is generated by the specified parameters. The difference between the generated reference and the load current determines the increment of the switching interval. The ratio of the increment of switching interval to the error signal is 4.4 μsec/digit. In other words, the base digits in the 8-bit down counter are changed by 2 digits/A. Then the dynamic equations with the varied switching interval provides the two current values at the next time step. The simulation of the system dynamics for two intervals, periods of charging and holding, proceeds in the same way as that explained in the Section 7.1.

The waveforms of the reference, the storage, and the load currents are shown in Fig. 7.5(a), and the waveform of the switching interval is shown in Fig. 7.5(b). The reference signal rises with the rate of 25 A/sec until it reaches 75 A and then keeps the constant value. The phase differences are given as 39° and 5° for the current rise and the constant current periods, respectively. The switching interval varies within the two extremes, 222 and 333 μsec, started at 264.1 μsec. The time step is reduced to 0.04 sec.

A negative error signal at the beginning of the energy transfer period decreases the switching interval until reaching its minimum. Then, when the error signal becomes positive, the switching interval becomes increased until reaching its maximum. The load current varies very slowly by frequency modulation. In an experiment, referred to in Section 6, the more rapid change of the dc voltages, corresponding to that of the switching interval, is observed. At the converter frequency of 631 Hz, about 25 control computations in one time step are possible. The slow response of the load current to the reference signal may be due to the insufficient time step. For a constant current period, the load current remains constant while the switching interval is decreased.

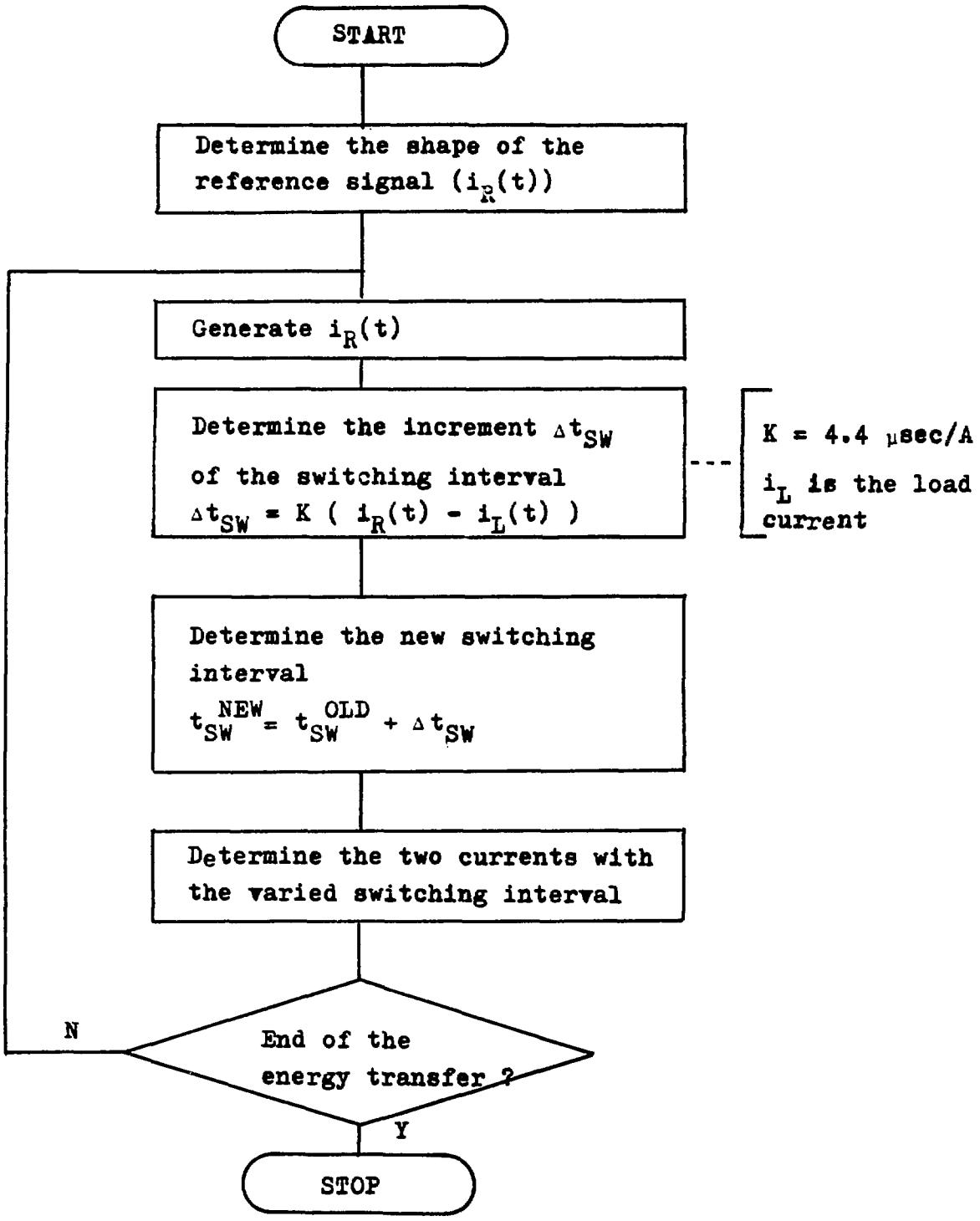

Fig. 7.4. Flowchart of the feedback control method by frequency modulation.

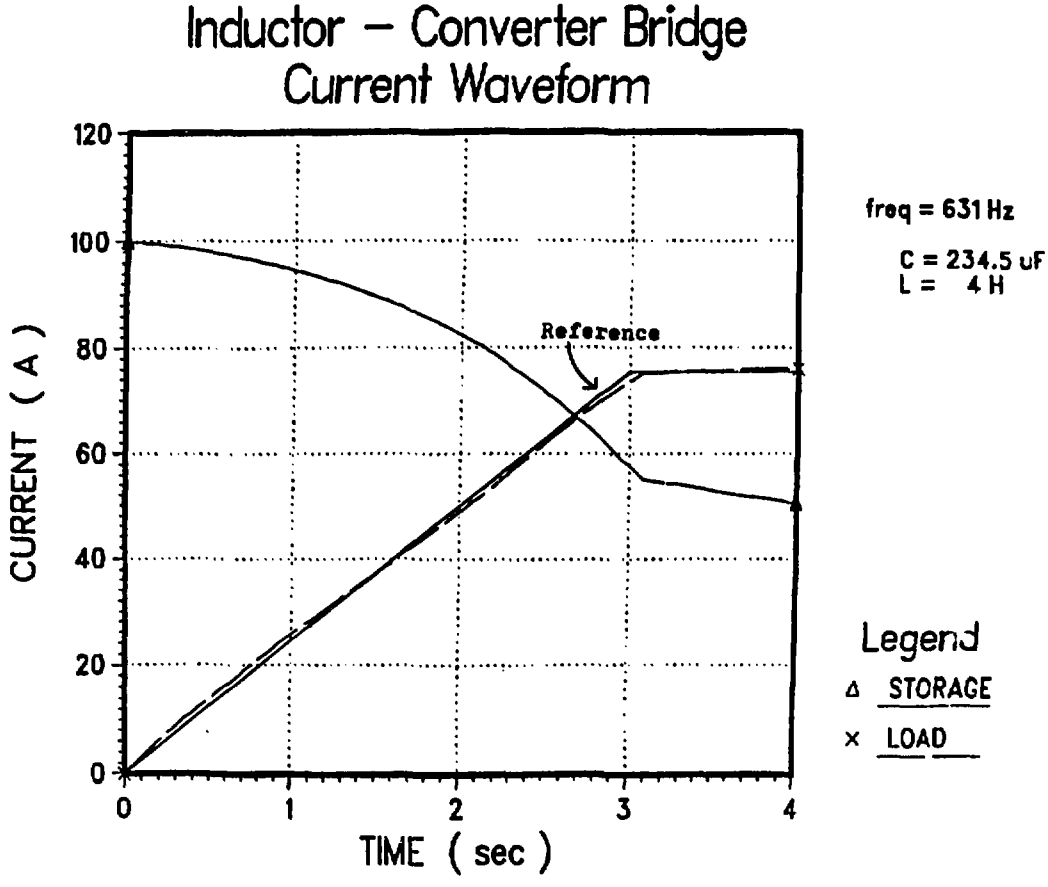

Fig. 7.5. Simulation of the feedback control method by frequency modulation.

(a) Waveforms of the reference, storage, and load currents.

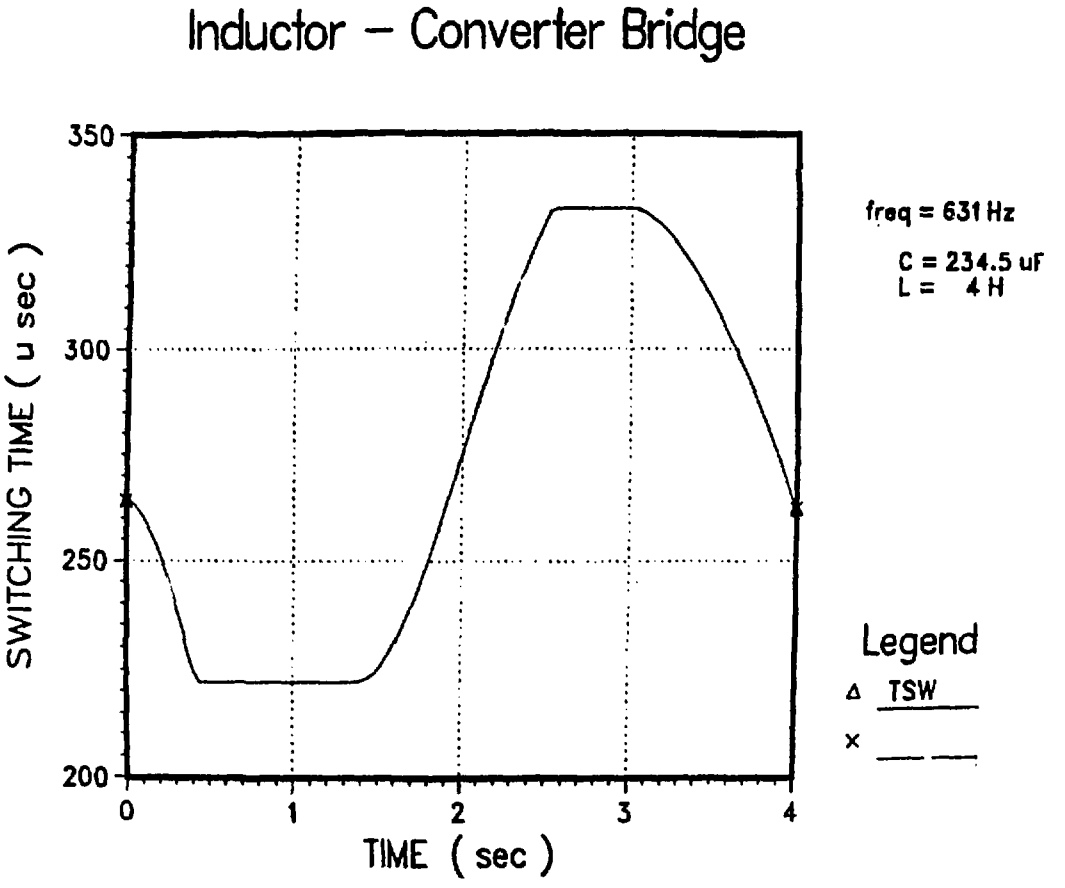

Fig. 7.5. Simulation of the feedback control method by frequency modulation.

(b) Waveform of the switching interval.

7.3 Two-Input Control System

For the modified open-loop control method, the phase difference is determined from the computation of the control equation with the feedback storage current. For the feedback control method by frequency modulation, the increment of the switching interval is determined by the difference between the reference and the load currents. Two control methods can be applied at the same time to regulate the load current. Figure 7.6 shows the block diagram of the two-input control system. The reference signal waveforms are characterized by the two intervals, periods of charging and holding. The switching interval and the rate of the current rise in the coefficient, α, are fixed during the energy transfer period. The phase difference and the increment of the switching interval are independently determined.

Figure 7.7 shows the flow chart of the two-input control system. The necessary parameters for determining the shape of the reference signal are initially specified. The phase difference is determined from the control equation using the storage current, while the increment of the switching interval is determined from the difference between the generated reference and the feedback signals. Then the storage and the load currents at the next time step are provided by the dynamic equations with the varied phase difference and converter frequency.

Figure 7.8(a) shows the two current waveforms. The reference signal rises with 25 A/sec until it reaches 75 A. Its waveform overlaps the load current waveform. The time step is further decreased to 0.02 sec. Figure 7.8 (b) and (c) show the waveform of the phase difference and the switching interval, respectively. During the current rise period, the phase difference is increased until the load current reaches 75 A. The fundamental waveform of the switching interval is gradually increased with an oscillation. The increased switching interval provides the additional energy transfer and reduces the difference between the reference and the load currents.

The characteristics of the two-input control method are the following:

1. The modified open-loop control method determines the fundamental waveform of the load current. The feedback control method by frequency modulation reduces the difference between the reference and the load currents. Then, by combining the two control methods, we

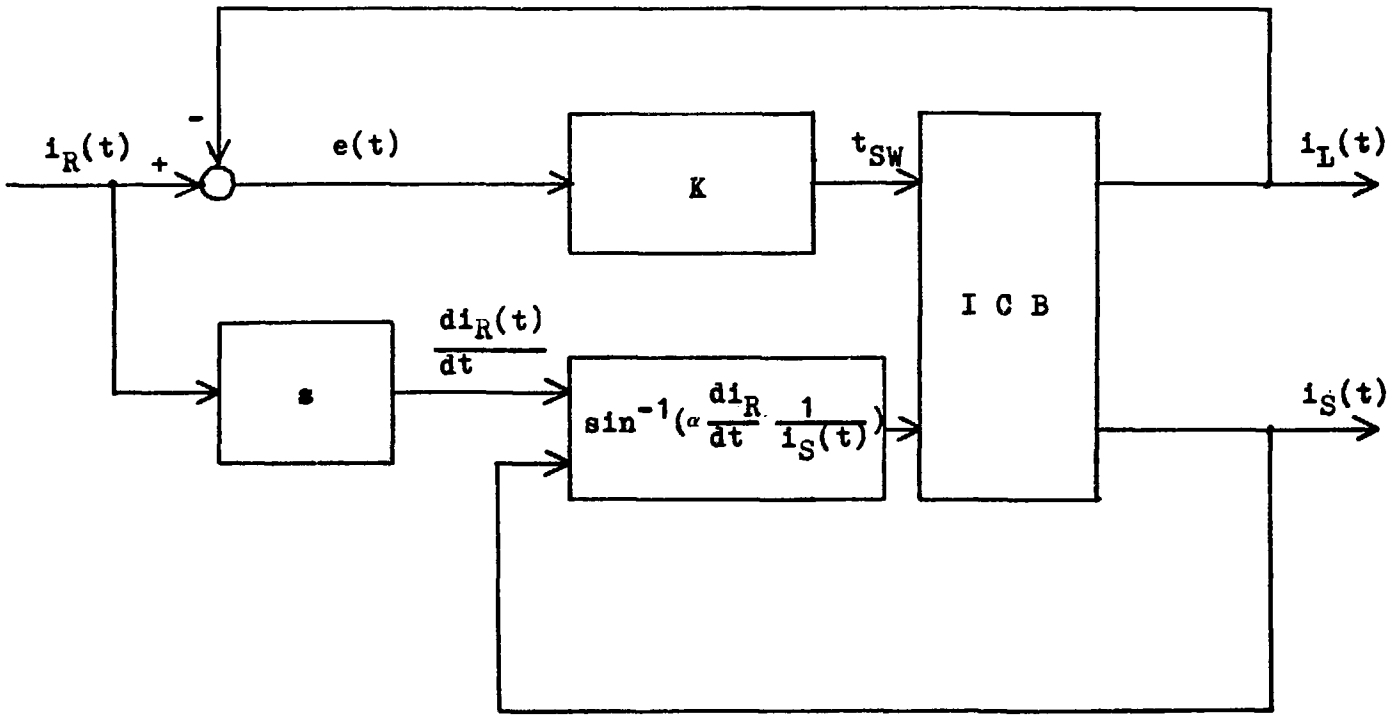

where $\alpha = \frac{\pi^3 CL_L}{54\ t_{sw}}$, K = 4.4 μsec/A

Fig. 7.6. Block diagram of the two-input control system.

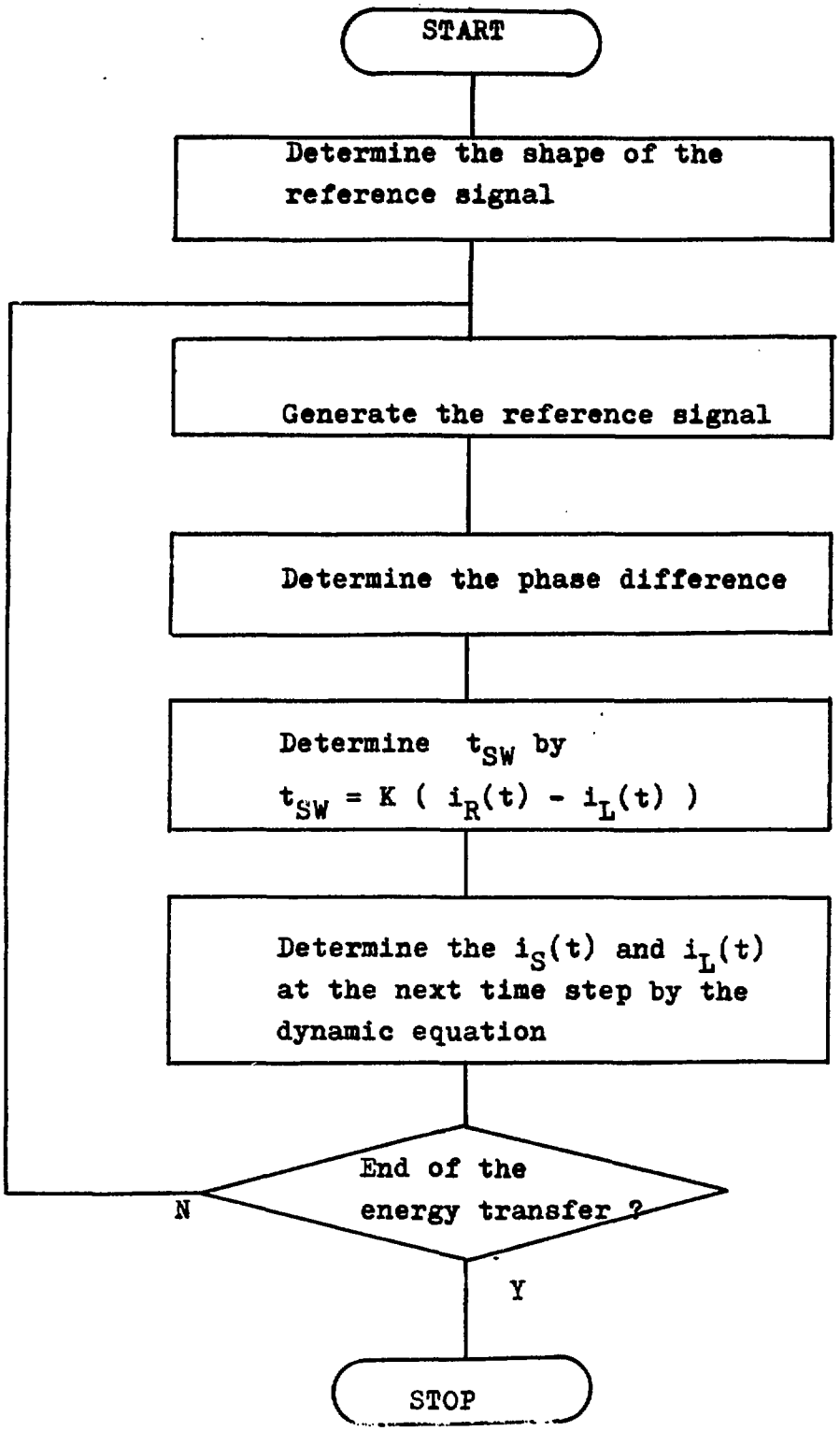

Fig. 7.7. Flowchart of the two-input control method.

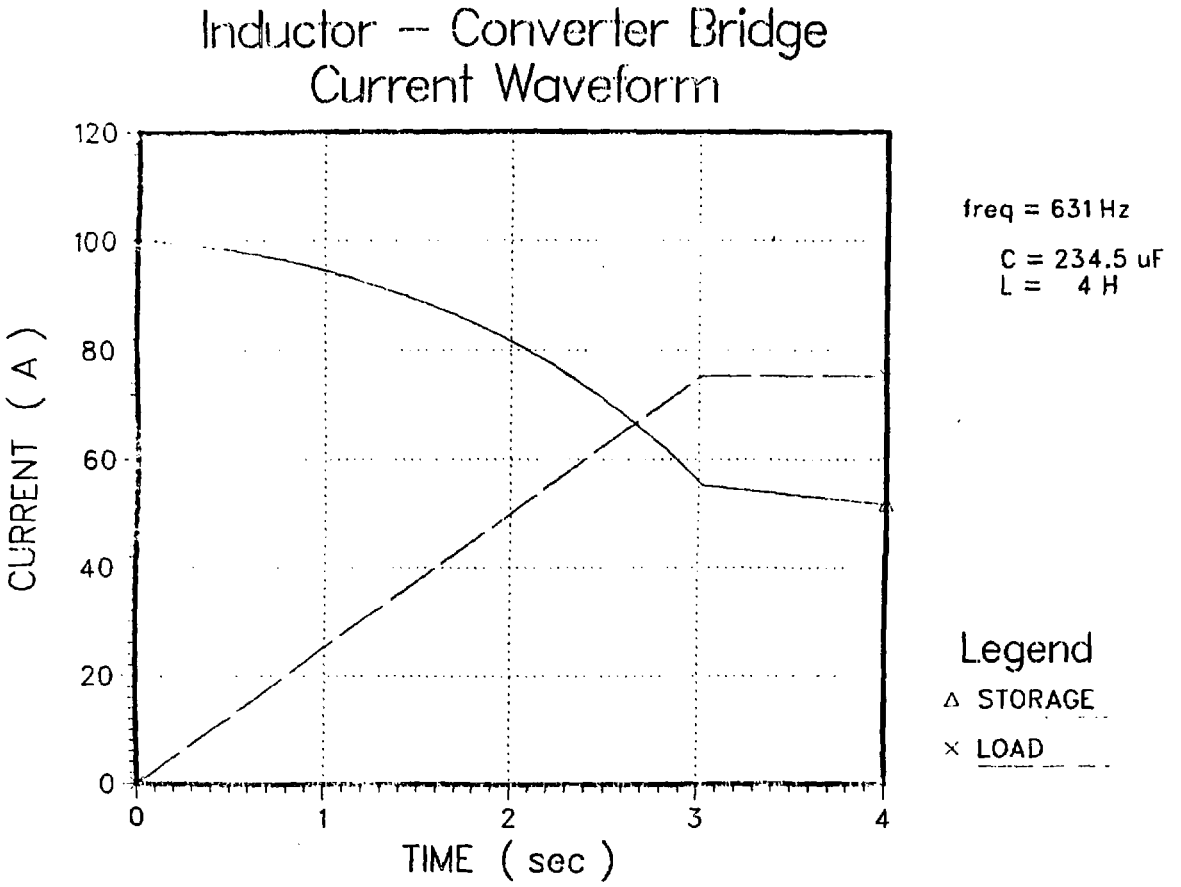

Fig. 7.8. Simulation of the two-input control method.

(a) Waveforms of the storage and the load currents.

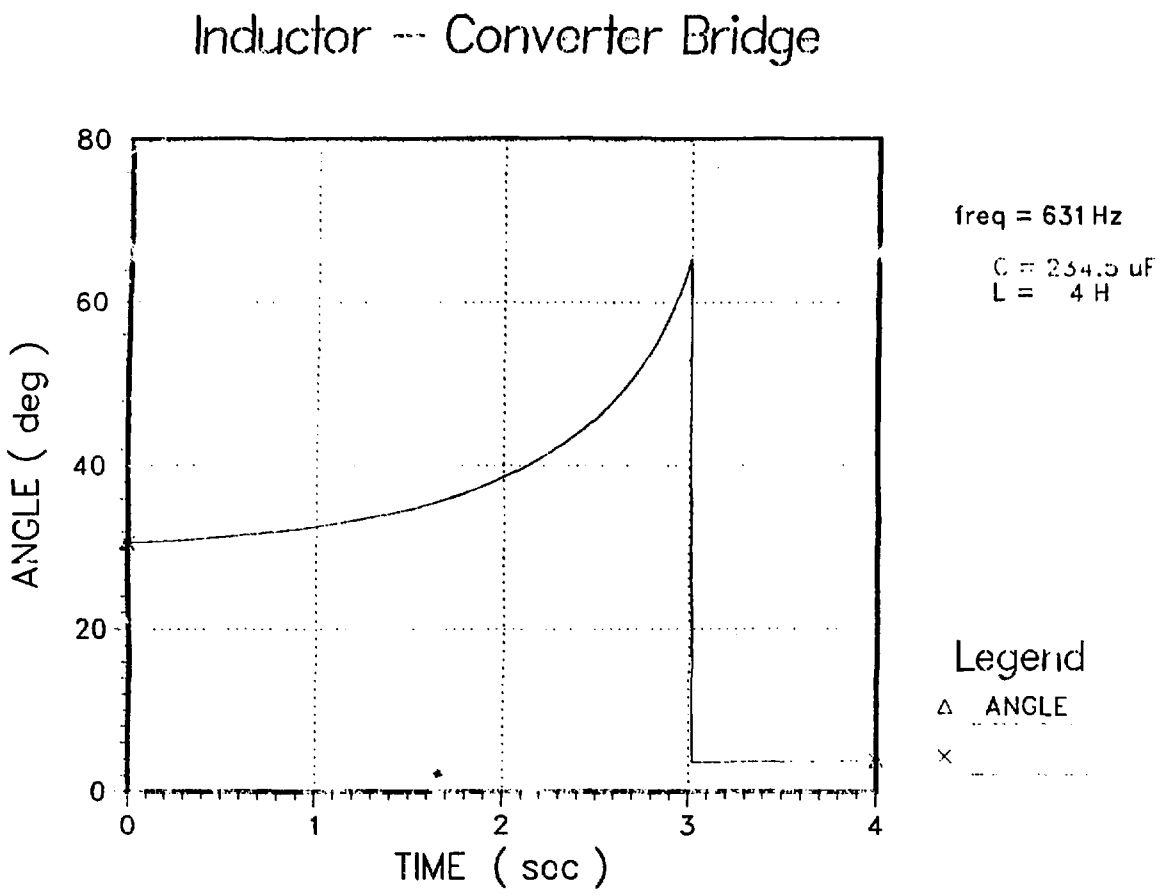

Fig. 7.8. Simulation of the two-input control method.

(b) Waveform of the phase difference.

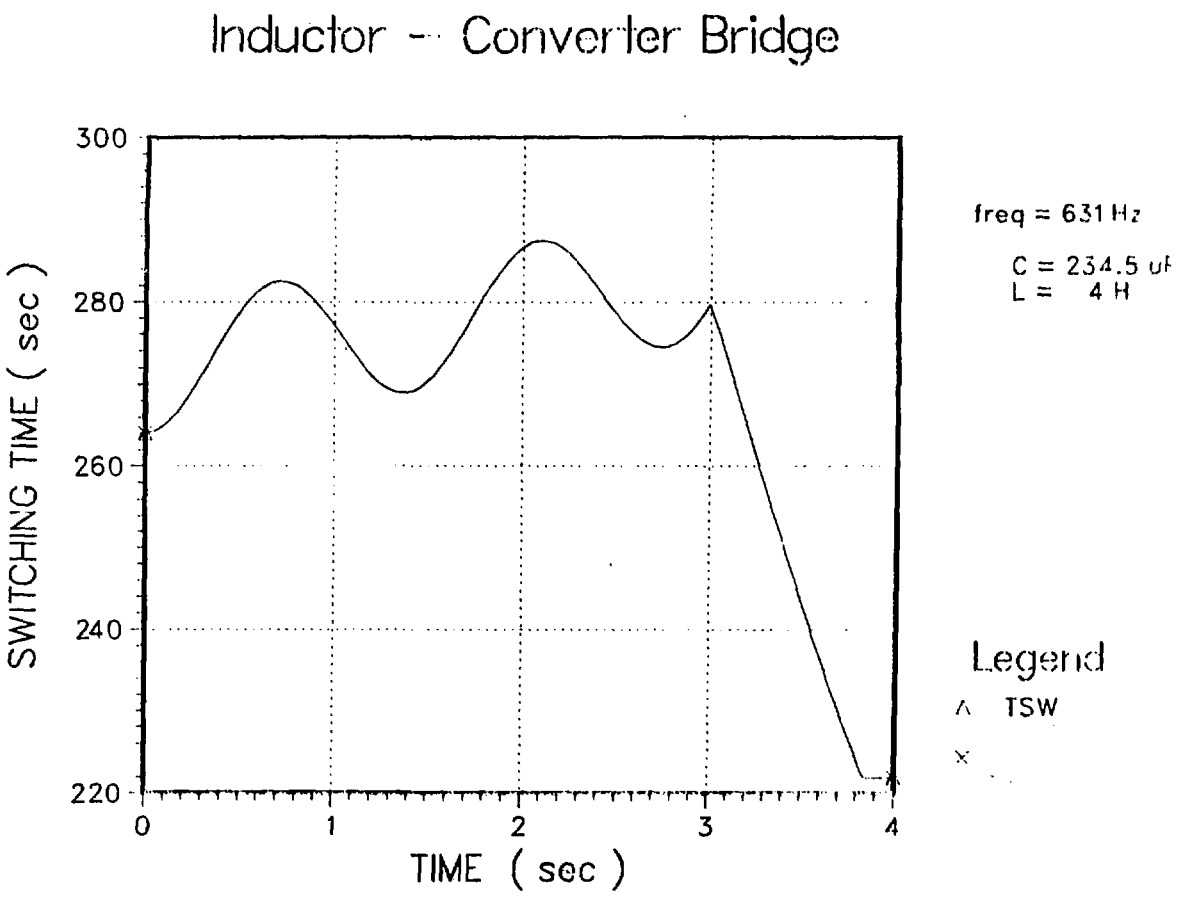

Fig. 7.8. Simulation of the two-input control method.

(c) Waveform of the switching interval.

can obtain the control system, the output of which varies within a limited range without the large magnitude of the voltage oscillation.

2. If the bang-bang control method is implemented with frequency modulation, it only provides the voltage swing within a limited range. Therefore, the effect of the voltage oscillation on the system performance, discussed in Section 4, is reduced.
3. The phase and the frequency may be regulated at the same time without deteriorated control performance. However, the frequency modulation method needs further study.

8. Conclusions

The main objective has been the design of a control algorithm for the three-phase prototype inductor-converter bridge. The fundamental work on the mathematical description of the inductor-converter bridge and the bang-bang control method was started by Ehsani.[9] We further develop the mathematical description and discuss the bang-bang control method. In addition to the supplement of the previous work, we introduce the modified open-loop control method and examine the possible implementation of the frequency modulation method. We simulate the system dynamics by the modified open-loop control method and by the feedback control method with frequency modulation. We also simulate the two-input control method as a future development and verify the possibility of good control accuracy by this method.

The following results are summarized:

(1) Considering that most of the net power is delivered at the fundamental frequency, we express net power of the capacitor bank in terms of the storage and the load currents. For the process of power flow from the storage unit to the capacitor bank and from the capacitor bank to the load unit, we obtain the dynamic equations, including the energy loss terms:

$$\frac{di_S(t)}{dt} = -\frac{54\, t_{sw} \sin\phi}{\pi^3 C L_S}\, i_L(t) - \frac{R_S}{L_S}\, i_S(t) - \frac{2V_f}{L_S},$$

$$\frac{di_L(t)}{dt} = \frac{54\, t_{sw} \sin\phi}{\pi^3 C L_L}\, i_S(t) - \frac{R_L}{L_L}\, i_L(t) - \frac{2V_f}{L_L}.$$

Energy loss takes place due to the wiring resistance, the thyristor forward voltage drop, and thyristor switching. The resistive and the thyristor forward voltage drop loss are expressed in terms of the storage and the load currents. On the other hand, the thyristor switching loss is difficult to express in terms of two currents because many factors contribute to the thyristor switching mechanism.

(2) We discuss the performance of the inductor-converter bridge by the bang-bang control method. The load current rises very smoothly, although the dc voltages at both converters oscillate from one extreme to the other. Noise increases the voltage oscillation. Then the low pass filter is placed between the dc current transformer and the A/D converter. If the voltage swing, relevant to the bang-bang control method, does not devastate the system performance, this control method may be suitable for the controller of the inductor-converter bridge.

The magnitude of the switching voltage varies with the phase difference and the current ratio. Moreover, the highest switching voltage exists during the transient period of the phase shift. This fact is a typical characteristic of the current source system.

(3) The control equation for the modified open-loop control method is derived from the dynamic equation. The phase difference is expressed as a function of the storage current. In a control computation process, the phase difference is determined by searching a stored list of phase difference corresponding to storage currents. The experimental results show that load current rises without any oscillation. This method provides a constant rise of the load current as long as the phase difference stays within two extremes, $-90°$ and $90°$.

The control equation for the constant current period does not provide enough energy transfer to keep the load current constant. The droop of the load current may be due to the uncertainty of the specified loss parameters.

(4) We control the load current by the frequency modulation method. There exists some limitations on the frequency modulation method with the present hardware due to the method itself and to the present hardware performance.

The frequency shift requires the control of the two pulse sequencers. But the computer is only allowed to control one of the two pulse sequencers at one time. Then, after the transient period of the frequency shift, the additional phase shift is created by the delay of the control from one pulse sequencer to another.

The change of the base digits in the 8-bit down counter alters the number of the increment of the switching interval. The relation between the base digits and its increment restricts the available switching interval because the hardware only accepts the integer numbers. The difference between the reference and the feedback signals determines the size of the increment in the switching interval. Then the system with a linear controller produces a slow current oscillation. The distortion on the current oscillation may be due to the insensitivity of the digitized error signal. From the experiment we verify the controllability of the energy tranfer rate by frequency modulation.

(5) We develop a dynamic simulation model by adjusting the energy loss terms. The values in a simulation are 0.1 Ω and 1.5 V for the wiring resistance and the thyristor forward voltage drop, respectively. At a low phase difference, there exists a relatively wide difference between an experimental and a simulated result at the end of the energy transfer period. But, in general, the simulation model may satisfactorily describe the experimental performance. By using this dynamic model, we simulate the performance of the inductor-converter bridge by the modified open-loop control method and by the feedback control method with frequency modulation.

As a future development, the two-input control method will be implemented. The phase shift provides the fundamental waveform of the load current, while the frequency shift compensates for the energy loss. We combine the two control methods and simulate the system dynamics.

References

1. T. H. Geballa and J. K. Hulm, "Superconductor in Electric Power Technology," Scientific American, Vol. 243, No. 5 (November, 1980).

2. R. L. Kustom, Thyristor Networks for the Transfer of Energy between Superconducting Coils, University of Wisconsin Press (1980).

3. H. A. Peterson, et al., "Superconductive Inductor-Converter Units for Pulsed Power Loads," Proc. International Conference on Energy Storage, Compression and Switching, Asti-Trino, Italy (November, 1974).

4. N. Mohan and T. Broach, "Converters for Supplying Pulsed Power Loads," IEEE Trans. on Industry Applications, Vol. IA-15, No. 1 (January/ February, 1979).

5. F. E. Mills, "The Fermilab Cryogenic Energy Storage System," IEEE Trans. on Magnets, Vol. MAG-11, No. 2 (March, 1975).

6. H. Fujino, et al., "Energy Transfer between SMES and Pulsed Loads," Proc. US-Japan Workshop on SMES, University of Wisconsin, Madison (October, 1981).

7. Y. Murakami, et al., "0.5 MJ Superconducting Pulsed Magnet for Energy Storage," IEEE Trans. on Magnets, Vol. MAG-17, No. 1, p. 505 (January, 1981).

8. E. W. Kimbark, Direct Current Transmission, Wiley-Interscience (1971).

9. M. Ehsani, "Development, Analysis, and Control of the Inductor-Converter Bridge," Argonne National Laboratory, ANL/FPP/TM-144 (1981).

10. D. P. Atherton, Nonlinear Control Engineering, Van Nostrand, Reinhold, London (1975).

11. D. P. Atherton, Stability of Nonlinear Systems, Research Studies Press (1981).

12. K. Ogata, Modern Control Engineering, Prentice-Hall (1970).

13. B. C. Kuo, Digital Control Systems, HRW, Inc. (1980).

14. T. J. Barnard and R. L. Kustom, "Changing Frequency of the Three-Phase Inductor-Converter Bridge, Argonne National Laboratory, Student Report (August, 1979).

Distribution for ANL/FPP/TM-170

Internal:

M. Abdou
C. Baker
C. Boley
J. Brooks
F. Cafasso
R. Clemmer
D. Ehst
K. Evans
P. Finn
Y. Gohar
L. Greenwood
D. Gruen
A. Hassanein
C. Johnson
J. Jung
S. Kim
R. Kustom (5)
R. Lari
B. Loomis
S. Majumdar
R. Mattas
B. Misra
R. Nygren
J. Roberts
D. Smith
L. Turner
ANL Patent Dept.
FP Program (15)
ANL Contract File
ANL Libraries (2)
TIS Files (6)

External:

DOE-TIC, for distribution for UC-20 (108)
Manager, Chicago Operations Office, DOE
Special Committee for the Fusion Program:
S. Baron, Burns & Roe, Inc., Oradell, NJ
H. K. Forsen, Exxon Nuclear Company, Inc., Bellevue, WA
M. J. Lubin, Standard Oil Company of Ohio, Warrensville Heights, OH
G. H. Miley, University of Illinois, Urbana
P. J. Reardon, Princeton University
D. Steiner, Rensselaer Polytechnic Institute
K. R. Symon, University of Wisconsin-Madison
K. Thomassen, Lawrence Livermore National Laboratory